UNIVERSITY OF CALIFORNIA,
IRVINE

Ovarian Follicle Toxicity Due to Low Dose Gamma Radiation: Determination of Persistence of Oxidative Protein, Lipid, and DNA Damage

THESIS

submitted in partial satisfaction of the requirements
for the degree of

MASTER OF SCIENCE

in Environmental Health Sciences

by

Stephen Craft

Thesis Committee:
Professor Ulrike Luderer, Chair
Professor Charles Limoli
Professor Stephen C. Bondy

2023

TABLE OF CONTENTS

LIST OF FIGURES

LIST OF TABLES

LIST OF ABBREVIATIONS

4-HNE	4-Hydroxy-2-Nonenal
ANOVA	Analysis of Variance
BER	Base Excision Repair
CDC	Centers for Disease Control
DDR	DNA Damage-Response
DNA	Deoxyribonucleic Acid
DSB	Double-strand Break
ESD	Effective Sterilizing Dose
EPA	Environmental Protection Agency
y	Gamma
GCR	Galactic Cosmic Ray
Gy	Gray
HZE	High-Energy Heavy Ions
HR	Homologous Recombination
IF	Immunofluorescence
IHC	Immunohistochemistry
ICRU	International Commission on Radiation Units and Measurements
ICRP	International Commission on Radiological Protection
SI	International Standard
IR	Ionizing Radiation
IACUC	Institutional Animal Care and Use Committee
LD50	Lethal Dose for 50% of an Exposed Population
LET	Linear Energy Transfer
LEO	Low Earth Orbit
KeV	Kiloelectron Volt
MVH	Mouse Vasa Homolog
NASA	National Aeronautics and Space Administration
NCRP	National Council on Radiation Protection
NHEJ	Nonhomologous End-joining
NTY	Nitrotyrosine
OSHA	Occupational Safety and Health Administration
PEL	Permissible Exposure Limit

PUFA	Poly-unsaturated Fatty Acids
ROS	Reactive Oxygen Species
RBE	Relative Biological Effectiveness
REID	Risk of Exposure Induced Death
SEP	Solar Energetic Particles
Sy	Sievert
SSB	Single-strand Break
USNRC	United States Nuclear Regulatory Commission
WR	Radiation Weighting Factors

ACKNOWLEDGEMENTS

I would like to express my sincere gratitude to my thesis committee chair, Professor Ulrike Luderer, and the members of my committee, Professor Charles Limoli and Professor Stephen Bondy, for providing their direction and expertise in the completion of this research project as this would not have been possible without their generous and unwavering efforts. I would further like to thank them for their mentorship throughout the Environmental Health Sciences graduate program and the Occupational and Environmental Medicine residency program at UC Irvine. Finally, I would like to thank Dr. Alya Khan, the residency program director, for her consistent encouragement, mentorship, and support which ultimately made it possible to complete this project.

ABSTRACT OF THE THESIS

Ovarian Follicle Toxicity Due to Low Dose Gamma Radiation: Determination of Persistence of Oxidative Protein, Lipid, and DNA Damage

By

Stephen Craft

Master of Science in Environmental Health Sciences

University of California, Irvine, 2023

Professor Ulrike Luderer, Chair

In November 2022, Artemis I successfully tested transport and automated docking systems for future missions that will ultimately usher in a new era for the United States National Aeronautics and Space Administration (NASA) and deep space exploration to Mars and beyond (1,2,3). Exposure to radiation in the form of galactic cosmic radiation (GCR) is likely one of the most dangerous of the five categories of hazards to be encountered by astronauts as we begin exploration beyond the Earth's protective geomagnetic fields (7). GCR is known to cause damage to ovarian follicles resulting in sterility and other related reproductive health problems, and with forty percent of the current 2021 Class of NASA astronauts consisting of female astronauts, a large portion of the team would be at risk (5,7).

In this study, we sought to build on previous research by quantifying the effects of dose-dependent gamma (γ) radiation on persistence of ovarian follicular oxidative lipid, protein, and DNA damage. This data will provide valuable comparison data for future studies looking at an overall mechanistic model and investigations into mixed-ion exposure effects like those encountered by astronauts in deep space exploration.

Methods: Three-month-old C57BL/6J female mice were exposed to γ-radiation at doses of 0, 15, or 50cGy at the UCI Department of Radiation Oncology cesium 137 source. Subject mice were euthanized one week after exposure and one ovary was fixed and stained for ovarian follicle counts. The other ovary was fixed for immunostaining using 4-Hydroxy-2-Nonenal (4-HNE), phosphorylated histone H2AFX (γ-H2AX), and nitrotyrosine (NTY) antibodies to identify oxidative lipid, double-strand DNA breaks, and protein damage respectively. Follicles with immuno-positive and negative oocytes and granulosa cells were counted and the percentages of positive follicles were calculated. We hypothesized that γ-radiation will cause a positive linear dose-dependent persistence of ovarian follicular oxidative stress at all follicular maturation stages.

Results: 137Cs y-radiation induced a general trend towards significance for dose-dependent persistence of oxidative lipid damage in granulosa cell positive primary and secondary follicles when directly comparing the 0cGy and 15cGy dose groups and oocyte positive primordial and primary follicles when directly comparing the 0cGy and 15cGy dose groups. Positive dose-dependent persistence of double-strand DNA damage also trended towards significance in the 15cGy dose group for oocyte immunofluorescence staining when directly comparing primordial, primary, and secondary follicle maturation stages and primordial to secondary follicles for positive granulosa cell staining. Nitrotyrosine immunofluorescence staining for oxidative protein damage was ultimately inconclusive due to technical issues with the dual-antibody protocol.

Conclusions: Our data indicate that in vivo γ-radiation of mice does not result in dose-dependent increased persistence of dsDNA breaks and oxidative lipid damage in the ovaries at one week after irradiation. These findings are inconsistent with published data from heavy

oxygen and charged iron studies. Ultimately, further investigation could be completed with varied mouse genetic strains, increased testing iterations to increase the power of the study data, and additional dose groups to elucidate any possible dose-response relationship. Finally, the newly developed immunofluorescence protocol will greatly increase the speed and reliability of data acquisition for these types of studies in the future.

INTRODUCTION

Fifty-three years ago, NASA successfully landed the Apollo 11 crew and lunar module on the surface of the moon. In November 2022, Artemis I—the first of six Orion spacecraft—tested transport systems for future missions that will include sending the first female astronaut to the moon (1,2,3). These missions comprise the initial steps in testing NASA's Deep Space Exploration Systems with the goal of human spaceflight to Mars and beyond (2,3).

Exposure to radiation in the form of galactic cosmic radiation (GCR) is listed as likely one of the most dangerous of the five categories of hazards to be encountered by astronauts and are predominantly composed of protons, neutrons, helium ions, and ions heavier than helium (4,6). Of these, high charge and energy (HZE) ions represent the dominant component in terms of tissue level biological response and have been shown to produce different biological results in various body tissues when compared to similar exposures to terrestrial radiation sources (10,20,21). NASA astronauts are selected from thousands of applicants that volunteer to undergo rigorous physical testing and academic training to further the goals and missions of the United States in space exploration and to the greater benefit of society (11). Fundamentally, these astronauts are employees of NASA, and therefore all reasonable resources should be used to reduce radiation risks and exposures to the lowest achievable levels to create an overall risk profile like other accepted occupations with exposure to radiation environments (8,12). Current permissible exposure levels (PELs) for radiation exposure in astronauts are provided by the National Council on Radiation Protection (NCRP) and are expressed in terms of percent risk of exposure induced death (REID) from cancers and relative biological effectiveness (RBE) factors addressing organ specific non-cancer related morbidity and mortality with the former currently set at a 3% REID career dose limit (8,12). Estimates of duration of travel with current propulsion technology for a return trip to the moon with extended stay for further scientific

experimentation or eventually to deep space and Mars would take approximately one-hundred eighty days and three years respectively and incur ionizing radiation exposure to the astronauts at estimated doses from 0.17Sv to 1.07Sv with the latter exceeding the current NASA career dose limit (7,12,56).

According to Cucinotta and colleagues, larger possible errors in risk modeling also exist because these values are based on epidemiology studies of atomic bomb survivors, which examined hazards for terrestrial gamma (γ) radiation and assumed similar biological dose response of GCR's for both endpoints of total cancer related mortality and organ specific noncancer morbidity (9,10). Ongoing NASA research aims to improve the accuracy of these models by developing a more mechanistic research approach.

The 2021 Class of NASA astronauts is forty percent females, and some of the heavy ions that make up GCR's are known to cause damage to ovarian follicles, resulting in sterility and increased risk for cardiovascular disease, osteoporosis, and Alzheimer's disease (5,6). However, this remains a relatively understudied topic as it relates to risk modeling for prolonged space flight and deep space missions to Mars (7,8). We sought to build on previous research by quantifying the effects of low-dose gamma (γ) radiation on ovarian follicles of female mice to determine the dose related persistence of oxidative lipid, protein, and DNA damage for comparison with prior studies from Mishra et al. investigating similar endpoints at low doses following irradiation with single particle heavy oxygen or iron particles (6,62). This research will assist with further studies examining early markers for persistence of ovarian oxidative stress and other biological effects in mixed ion fields as well as help to create additional evidence for dose-response effects in a previously proposed mechanistic model for ovarian tumorigenesis (55). These investigations aim to improve the overall accuracy of modeling approaches for biological effects in mixed ion fields like those encountered by astronauts in deep space exploration.

CHAPTER 1: LITERATURE REVIEW

Radiation is defined by the Centers for Disease Control (CDC) as “energy from a source that travels through space at the speed of light” and notes it contains other characteristics such as an electric and magnetic field with “wave-like” properties (15). Radiation is broadly classified as non-ionizing radiation and ionizing radiation (IR). This research focuses on IR, which contains enough energy to dislodge electrons from their atoms (29). We are specifically concerned with the ability of IR to create different variations of cellular damage (15).

Much is known about radiation, beginning with Roentgen’s discovery of x-rays in the 1800’s, Heisenberg’s theory of quantum mechanics, and use of the atomic and hydrogen bombs in the mid 1900’s. In the mid-1900’s, the scientific community gained deeper understanding of the Earth’s magnetic field and its interplay with the surrounding Van Allen radiation belts, and now has continued to study solar radiation sources and HZE particles relative to deep space exploration (13,14,16). The United States Nuclear Regulatory Commission (U.S.NRC) defines radioactivity as the “amount of ionizing radiation released by a material”, but this definition can be misleading when determining the total risk estimation without a greater understanding of sources, exposure, dose, and dose equivalent effects because different sources create varying levels of biological change or damage depending on absorption and tissue specific interactions (17,19). According to the Occupational Safety and Health Administration (OSHA), there are six general types of ionizing radiation grouped into two categories based on presence or absence of mass and charge (34).

Particulate radiation contains measurable mass and charge and includes alpha particles (two protons and two neutrons), beta particles (negatively charged electrons), positrons (positively charged electrons), and neutrons (34). Electromagnetic radiation is absent of mass or charge, includes gamma rays (γ), known as photons, and consist of essentially pure energy emitted from the nucleus of a radioactive atom and X-rays, which are like gamma rays (γ) but originate from outside of the nucleus (34) (Figure 1).

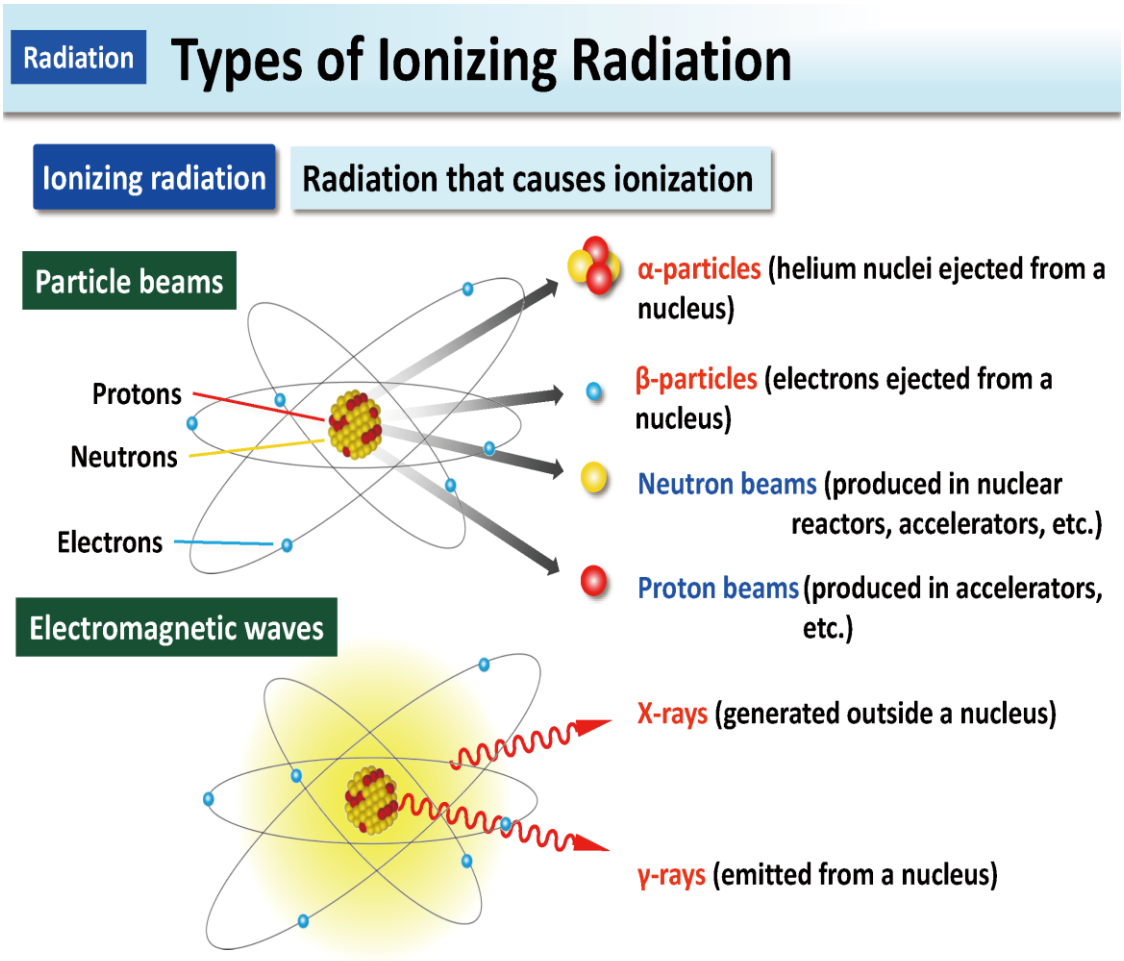

Figure 1: *Types of Ionizing Radiation. Image courtesy of ME of Japan (84).*

Common units of measurement of radiation were developed to more accurately describe or quantify the significant variables associated with the effects produced with various exposures and ultimately allow for improved generalized comparisons between sources and types of radiation when investigating the different tissues and organ systems being exposed. For the purposes of this study, the basic quantities of ionizing radiation include "absorbed dose, dose equivalent, and effective dose" and are referenced via current International Standard (SI) units (17,18). "Absorbed dose" is the general term for total energy deposited in any given tissue by a specific type of radiation per mass of the tissue and expressed by the SI unit gray (Gy) (18). This measurement is helpful for comparison of different types of radiation by evaluating the end energy absorption in a material resulting from various exposure types (18). "Equivalent dose" helps to quantify the absorbed dose related to effects on human tissues and is expressed by the SI unit sievert (Sv) (18). This unit introduces the concept of "relative biological effectiveness (RBE)" and considers different biology effects produced by the various sources of radiation on tissues at the same absorbed dose (18,20). The following formula is commonly utilized with D*x* representing the radiation source under study and D*ion* as the reference (36). The reference dose is in the numerator and is almost always the dose of 250 kVp x-rays to elicit a given biological effect. The test dose is in the denominator.

$$RBE = \frac{D_x}{D_{ion}} \quad (36)$$

Establishment of RBE will ultimately prove useful in increasing accuracy of extraterrestrial exposure risk stratification models when utilizing data from terrestrial exposure studies via application of programs such as the US Environmental Protection Agency (EPA) benchmark dose modeling which allows estimation of qualitative dose-response relationships (67).

Finally, “effective dose” aids in comparison of equivalent dosing weighted to biological harms in different types of specific tissues (18). This is also expressed by the SI unit of Sievert (Sv) and defines the dose equivalent which weights radiation types based on RBE. This one to evaluate specific radiosensitivity or biological harms experienced among different body tissues at any given absorbed dose from different radiation types (18).

It is estimated by leading experts that an astronaut traveling through deep space, such as a Mars exploration mission, will be exposed to several different types of ionizing radiation including GCRs and solar energetic particles (SEPs) with the former accounting for the majority of total absorbed dosage for such a mission. GCRs contain approximately 90% protons, 9% alpha particles, and 1% HZE ions lacking orbital electrons (lithium, carbon, oxygen, silicon, iron, etc.) with the latter representing the dominant component of tissue level biological relevance and inherent radiation exposure risk due to the high charge and mass of these elements (29,33,35,37,50).

Current risk models have adopted the assumption that during prolonged lunar or deep space missions, the spacecraft occupants will have essentially every cell in their body affected either by traversal of HZE ions or biological pathways that mimic radiation effects adjacent to the cells with direct damage from ionizing radiation (7,21).

It is also important to describe in more detail the specific types of damage caused by ionizing radiation exposures to include direct deoxyribonucleic acid (DNA) damage, indirect damage via creation of excess reactive oxygen species (ROS), resultant effects on the cellular microenvironment from adjacent undamaged cell signaling, and increased rates of carcinogenesis and degenerative diseases in the various organ systems (2,7,14,27,29).

Direct damage to the DNA double helix occurs when a high energy particle or ray directly contacts the phosphodiester backbone and creates a single-strand break (SSB), double-strand break (DSB), or combination of both while indirect DNA damage refers to the production of excess ROS such as superoxide anions or hydroxyl radicals via water radiolysis in close proximity (~3 nanometers) to the DNA sugar phosphate backbone (Figure 2,3) (25,28-31). The term "clustered" refers to when these types of damage occur within a few helical turns of the affected DNA structure which can complicate or disrupt endogenous repair mechanisms and will be discussed in subsequent sections describing these mechanisms (28,29).

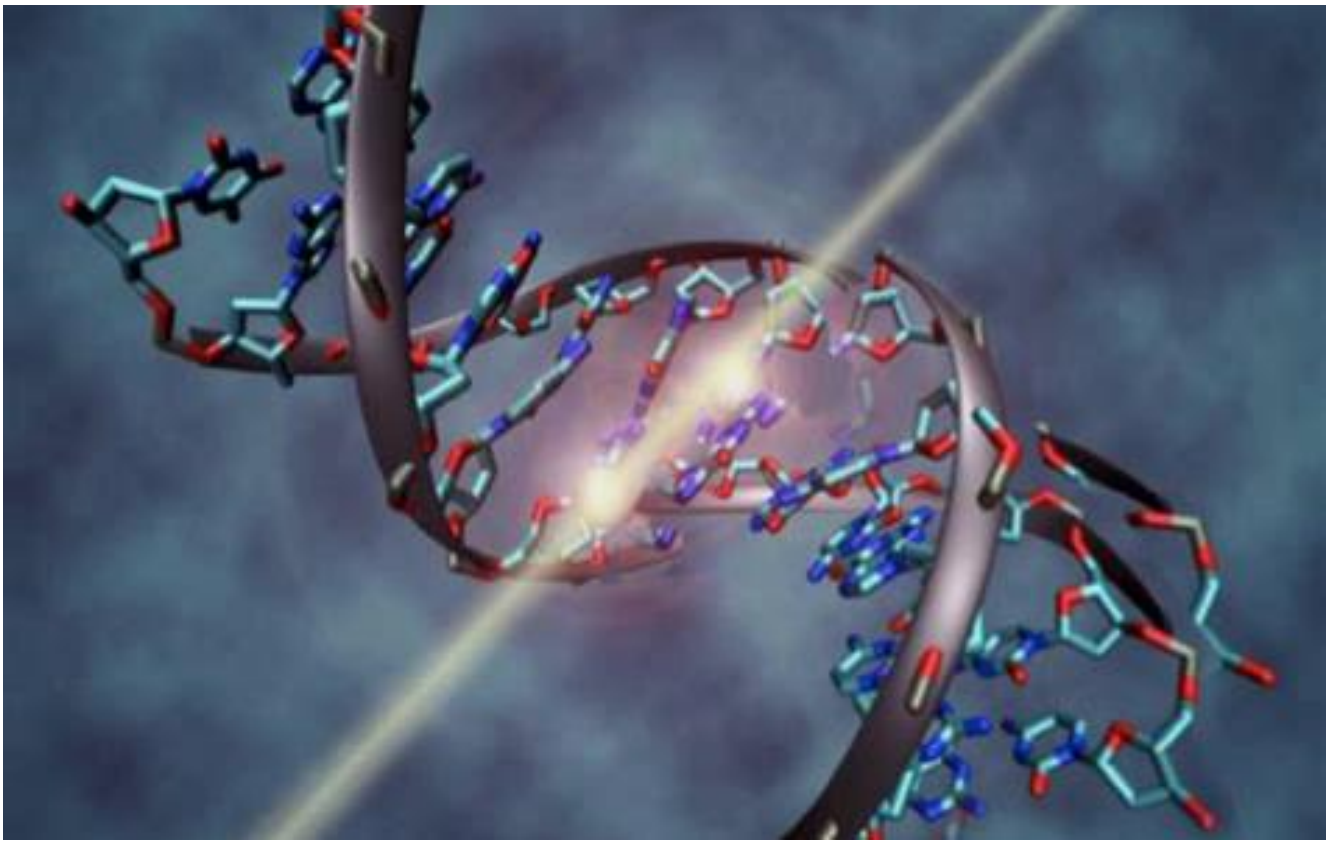

Figure 2: *DNA double helix damage. Image courtesy of NASA (86).*

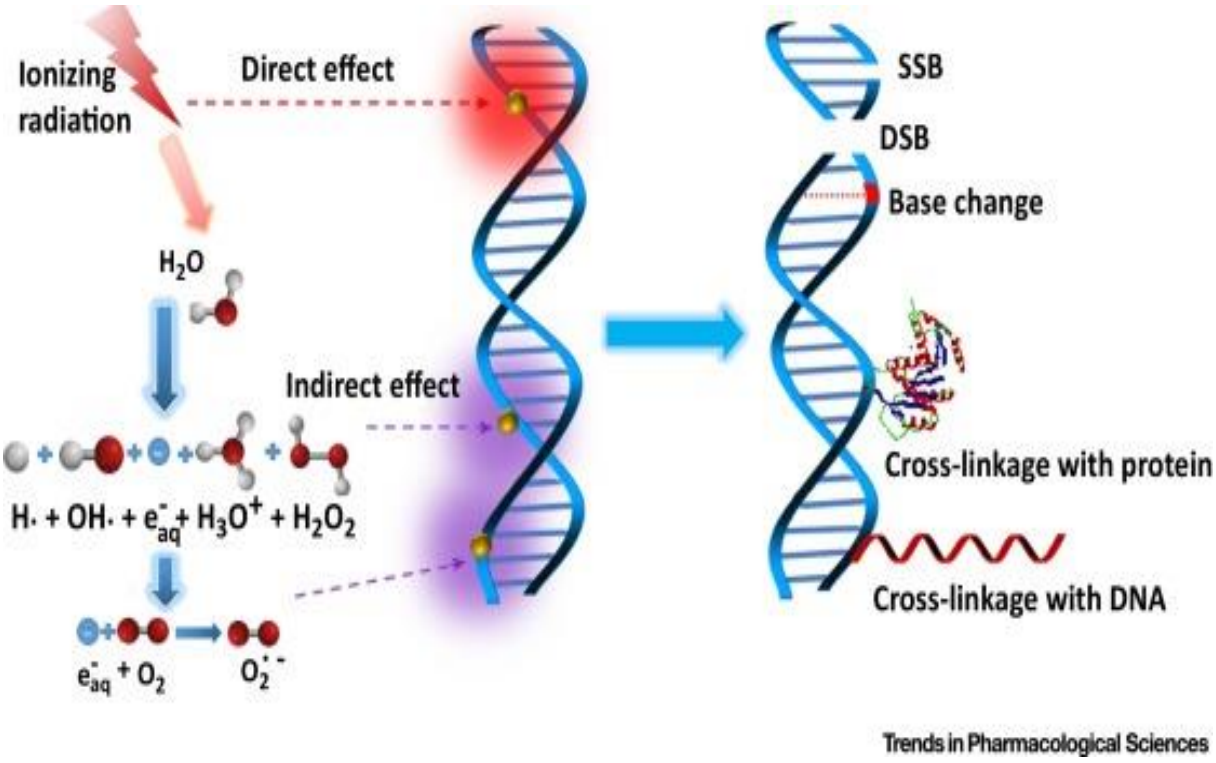

Figure 3: *DNA damage due to ionizing radiation. Image Credit: Wang, Hao, et al.,2018 (32).*

Researchers in radiation oncology have noted that approximately two-thirds of all radiation-induced DNA damage are the result of indirect exposure to IR via the increased prevalence of oxidative stress and pathologic generation of ROS in affected tumors and surrounding tissues (31). During normal cellular metabolism, ROS are produced in various sites throughout the cell with mitochondrial production comprising greater than 90% and specifically within the electron transport chain complexes (I, II, III) (31). The exact processes or downstream modulation related to the strict regulation of ROS production and neutralization is beyond the scope of this discussion, but it is a very precise system preventing unintended damage to cellular components such as DNA, RNA, proteins, and poly-unsaturated fatty acids (PUFA) (85). In the setting of IR induced production of ROS, these innate systems can become ineffective and allow for various simple and complex types of SSB or DSB damage to occur which can ultimately lead to increased risks of tissue death or carcinogenesis and has

become the nidus for extensive research investigating potential dietary strategies utilizing various mixtures of micronutrients administered both prior to and post-irradiation to aid in prevention and mitigation of these indirect insults (92,93).

Biophysical models described by Cucinotta, Furukawa, and Nelson et al. show that different sources of ionizing radiation can have similar numbers of DNA strand breaks and cumulative oxidative damage but result in vastly different downstream biological effects based on the location, density, and complexity of the imposed damage (7,21,25). Unfortunately, these models often can depend on the reference tissues and have historically been inaccurate revealing the need for an additional measurement and standard unit to describe these differences. Linear Energy Transfer (LET) is defined by the International Commission on Radiation Units and Measurements (ICRU) as the energy transferred (ionization) to a material over any given distance traveled through the material and is reported via kiloelectron volts per micrometer (KeV/μm) (14, 22, 29). This construct becomes extremely important when considering the improved accuracy in risk modeling based on RBE as previously mentioned because different sources of IR with similar energies can produce extremely different patterns of damage with variances of tissue depth and unit volume of tissue penetrated (14,22,26). To further describe this concept, IR sources are grouped into two general categories based on overall spatial distribution for the respective linear energy transfer (LET) and consist of low LET (x-rays, γ-rays, etc.) with relative energies below 10KeV/μm and high LET (GCRs, SEPs, Radon, etc.) with relative energies above 10KeV/μm (Table 1) and further utilized by the International Commission on Radiological Protection (ICRP) via weighting factors to estimate the comparative cancer mortality risks associated with each type of exposure (24, 29, 50).

Ionizing radiation type	Common sources	Linear Energy Transfer (LET)*	% Annual Exposure **	Particle track	Damage clustering ±	Damage Hallmarks
Photons	Gamma rays & X-Rays	Low	~35%	High penetration, crooked track	≤10 lesions per cluster	Highly penetrating but sparse damage; Random distribution of DSBs
β particles						
Protons	Cosmic rays & radon emissions	High	~65%	Low penetration, straight track	≤25 lesions per cluster	Complex clustered lesions surrounding DSB; "Dirty breaks"; Non-random DSBs (average break size 2kbp); Lagging repair
α particles						
HZE ions						

Table 1: *Spatial damage distribution patterns of various ionizing radiation types. Image Credit: Cannan et al., 2015 (29).*

High LET ionizing radiation has generally been shown to produce very dense and non-uniform damage along the penetration track through the tissues (Figure 4) simultaneously producing an equivalent low LET uniform component or secondary track (Figure 5) due to delta rays being emitted adjacent to the particle track trajectory (29). These lower secondary LET interactions also damage the biologic material similar to photon irradiations. (7,24). The inability to effectively repair regions of clustered DNA damage (i.e., regions of high damage multiplicity) contributes to the increased RBE for high LET exposures at the same absorbed dose as a low LET exposure. RBE varies with particle LET, reaching a maximum at 100 keV/u, a strictly geometric consequence that links the spatial distribution of ionizing species to the size of the DNA helix. (29,50).

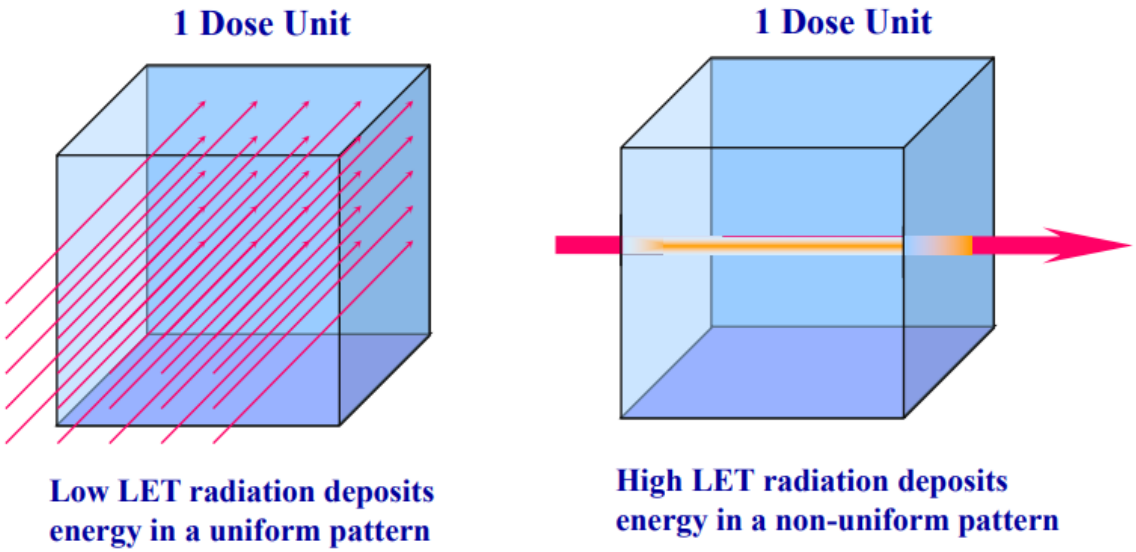

Figure 4: *Spatial distribution patterns of particles of various LET. Image Credit: Nelson, 2003 (25).*

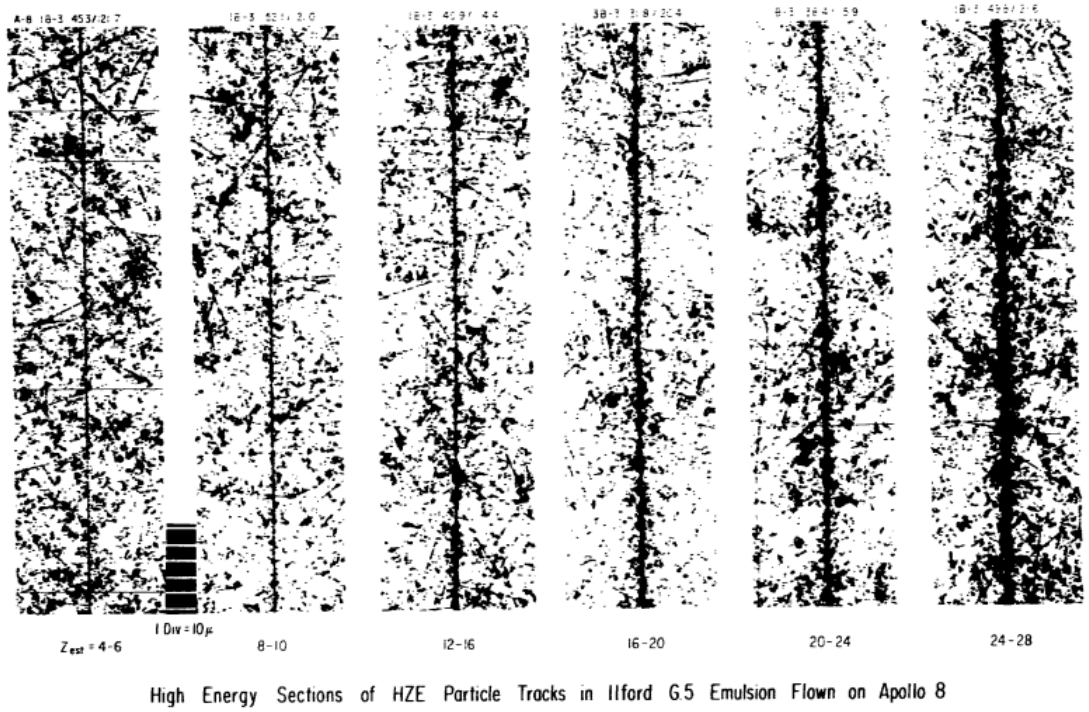

Figure 5: *Spatial distribution patterns of HZE particles of various charge. Image Credit: Schaefer et al., 1976 (23).*

Prior to further discussion regarding DNA repair mechanisms, it is relevant to briefly review the steps of the cell cycle where cells complete the normal cycle of cell growth and proliferation (21,39). The cell cycle is divided into several phases termed G_0, G_1, S, G_2, M (Mitosis), and Cytokinesis (Figure 6) (39,41). The phase G_1 is initiated via cell signals to grow and divide, and the process begins by replication of the intracellular components excluding the DNA. The S phase is also known as the synthesis phase and represents the portion of the cell cycle encompassing DNA duplication. The G_2 phase includes a second period of intracellular growth and reorganization but also contains several DNA error-checks and appropriate activation of mechanisms for those required error corrections. The M phase consists of several subunit phases required to separate the newly replicated DNA to allow for cytokinesis and appropriate genetic compliment to be transferred to each progeny cell. Finally, the G_0 phase represents a time when cellular division signaling is blocked and the cell remains quiescent. The cellular cycle has also been shown to affect a particular cell's relative sensitivity to damage from ionizing radiation in that a specified exposure administered or encountered during the G2-M phase will often be more deleterious to cellular DNA repair and ultimate survival than a similar dose encountered in the G1 phase and S phase respectively (88,89). This variable likely also contributes to an already multifactorial model in determination of radiosensitivity based on folliculogenesis stages or follicle size and how this potentially correlates heterogeneously even between mammalian species (90,91).

It is well known in the current literature that injured cells can undergo one of three pathways when exposed to IR and sustaining DNA damage to include repair of the damage via multiple DNA damage-response (DDR) systems, programmed cell death via apoptosis, or activation of DDR systems with incorrect or mismatch repair and persistent damage potentially increasing the risk of biophysical changes and potential carcinogenesis (19).

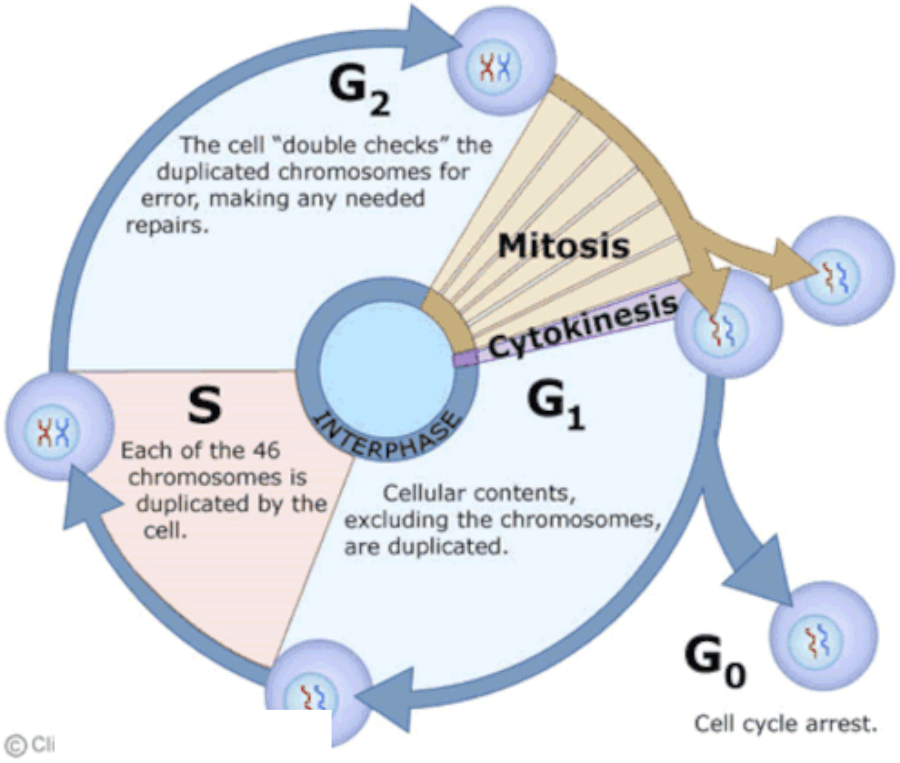

Figure 6: *The cell cycle, mitosis, and meiosis. Image Credit: University of Leicester (39).*

DDR systems are activated dependent on the type and source of various lesions to include SSBs and DSBs produced via exposure to IR and excess ROS with DSBs constituting the most severe damage to the cell. Various combinations of repair pathways exist to repair or correct these types of damage to include Base Excision Repair (BER), nucleotide excision repair (NER), homologous recombination (HR), single-strand annealing (SSA), and nonhomologous end-joining (NHEJ) (Figure 7) (31,44).

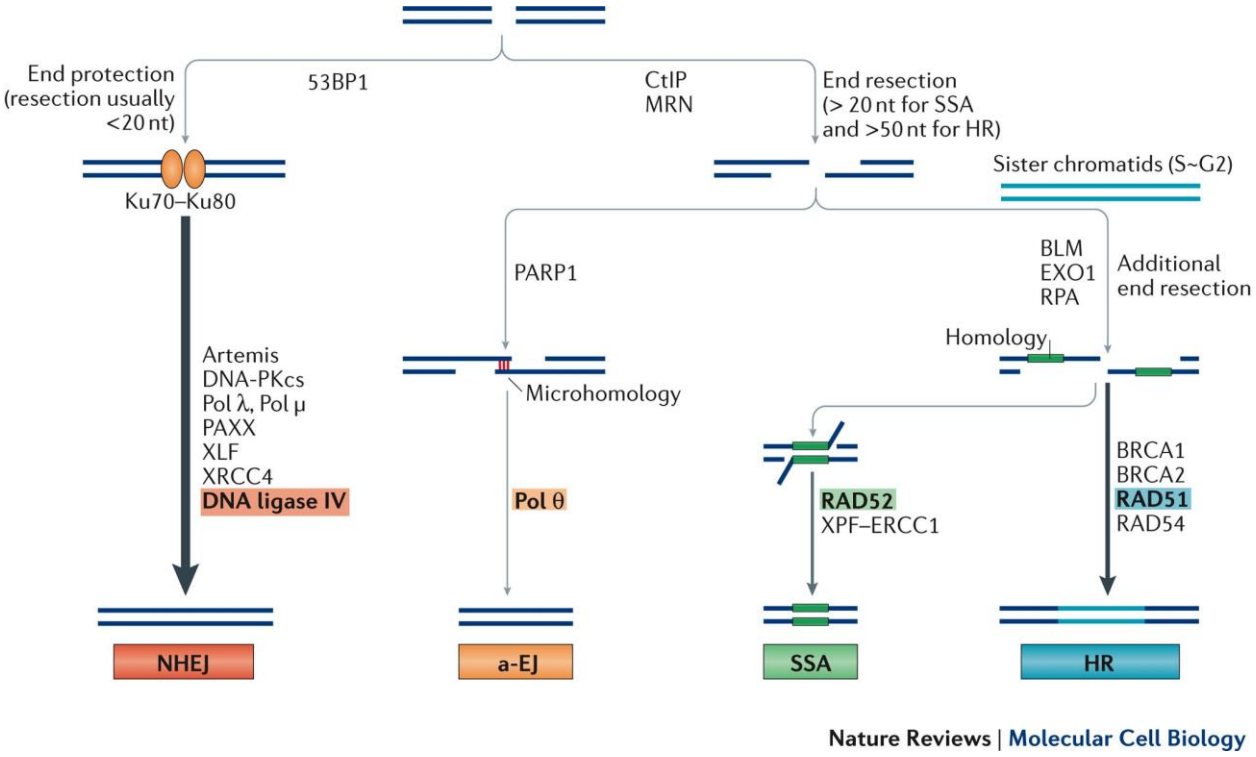

Figure 7: *Overview of DNA damage repair mechanisms. Image Credit Chang et al., 2017 (43).*

The exact mechanism utilized is dependent on multiple variables to include radiation dose, type and complexity of DNA damage induced, and cell cycle stage when damage occurs, but predominantly fall into either NHEJ or HR pathways with the latter more primary in cells involved in S and G_2 phases as this process utilizes the sister chromatid for a repair template. (21,29,28,40,43,44).

NHEJ occurs throughout the cell cycle and requires several gene products including a DNA-dependent protein kinase composed of a Ku70/80 heterodimer and adjoining DNA-PKcs, DNA ligase IV/XRCC4 complex, and several processing enzymes still under investigation (Figure 8) (43).

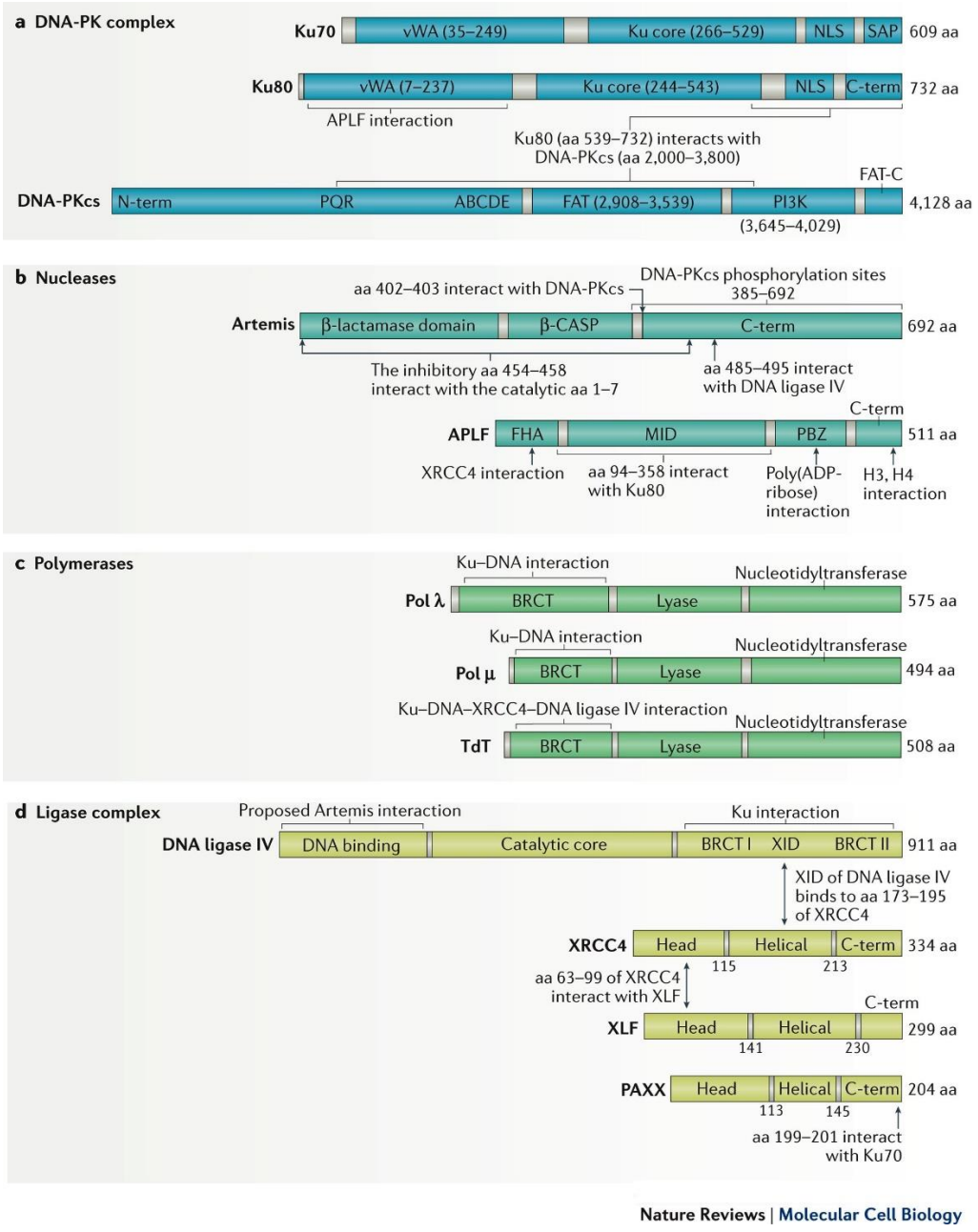

Figure 8: *Required gene products for non-homologous end joining. Image Credit Chang et al., 2017 (43).*

After IR exposure causes a DSB in a particular region of DNA, Ku70/80 then recognizes and binds to the DNA ends while recruiting and activating DNA-PKcs. Activated DNA-PKcs then binds the damaged ends and begins processing of non-complimentary strands and aids with recruitment of the DNA ligase IV/XRCC4 complex with final ligation and joining of repaired ends (Figure 9) (21,42,43,44).

Of note, this process often involves potential loss of nucleotides and is more error-prone in comparison to HR further preventing complete repair of the various types of DNA damage seen at the cluster sites created by exposure to high LET ionizing radiation (21).

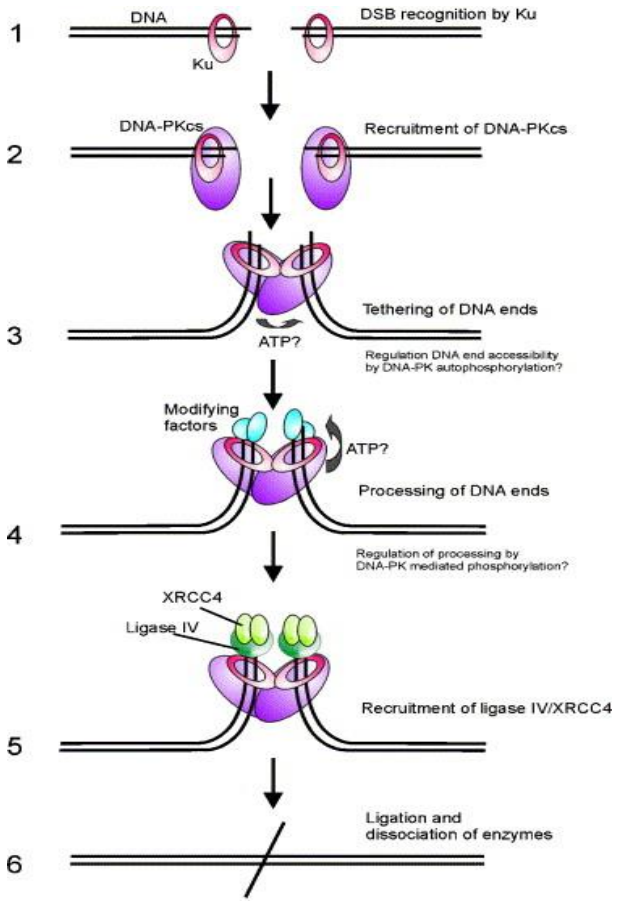

Figure 9: *Steps of non-homologous end joining. Image Credit Weterings et al., 2004 (42).*

In HR, (Figure 10) a non-damaged donor sequence is copied to the site of DNA damage in three overall processes or stages. The first stage entails the initial recognition and recruitment of a protein complex called MRN at the site of the IR induced DNA DSB. End resection by CtIP, Exo1, or Dna2 is then initiated to produce several 3′ single-strand tails which bind to replication protein A (RPA) (21,46,47).

The second stage involves displacement of the RPA complex, and the attachment and coating of the newly resected ssDNA ends by a protein RAD51 (21,45). This protein functions to invade the complimentary intact DNA strand generating a displacing strand (D-loop) which is utilized as the new repair template connected by two holiday junctions (21,45). Finally, the postsynaptic stage can involve multiple pathways to resolve the holiday junctions resulting in various cross-over and non-crossover products that are templated and essentially error free (21,46,48).

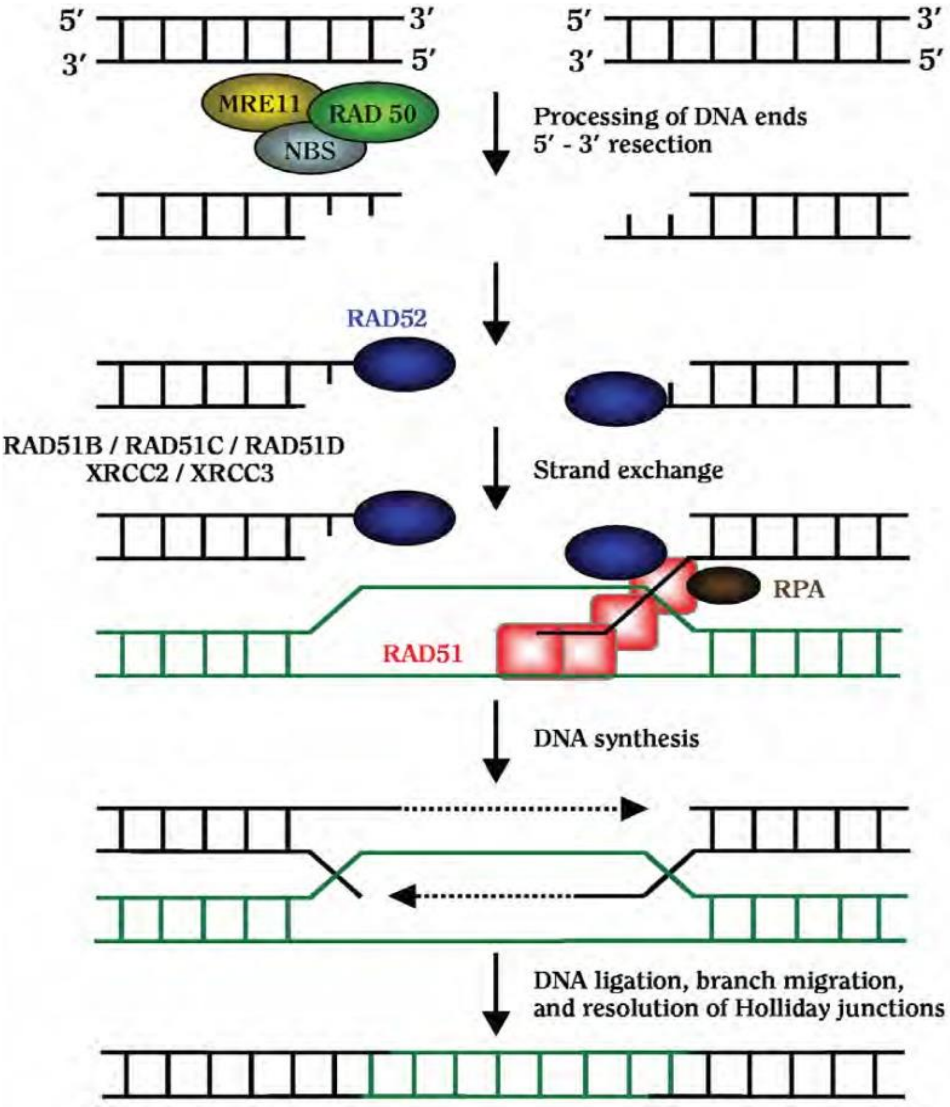

Figure 10: *Proposed steps of homologous recombination. Image Credit CDCaP, 2010 (49).*

Now that the underlying biophysical effects of IR have been introduced, discussion can be initiated regarding current risk mitigation models. NASA's space permissible exposure limits (SPEL) for space flight radiation exposure are the current NASA medical radiation permissible exposure criteria for astronauts (Table 2) and are like those of other international space agencies except for differences on age and gender (51). The updated 2022 proposed NASA SPEL standards will remove the age and gender restrictions for all astronauts and will still utilize data from low earth orbit (LEO), epidemiology data from atomic bomb survivors, and estimated 3% REID from post-exposure cancers (50,57).

Space agency	**Age at exposure (years)**				
Empty Cell	**Gender**	**30**	**40**	**50**	**60**
NASA	M	0.78	0.88	1.00	1.17
	F	0.60	0.70	0.82	0.98
JAXA	M	0.60	1.00	1.20	1.20
	F	0.60	0.90	1.10	1.10
ESA	M/F	1.00	1.00	1.00	1.00
RSA	M/F	1.00	1.00	1.00	1.00
CSA	M/F	1.00	1.00	1.00	1.00

Table 2: *Career effective dose limits (Sv) for astronauts in LEO. Image Credit Walsh et Al. (57).*

Many uncertainties still exist in the above models and more research needs to be done with a focus on female reproductive health to further characterize the potential for ovarian toxicity and other major reproductive organ pathology induced by GCRs exposure during deep space missions (50). It is well documented that overall radiosensitivity is mitigated by multiple variables and cellular reproduction frequency increases the deleterious effects of exposure to ionizing radiation (38). Specific cells in the female reproductive tract undergo increased replication rates such as during folliculogenesis in the mammalian ovaries. The basic ovarian follicular cycle consists of three main steps to include

initiation, follicle growth, and maturation of the follicle prior to ovulation with our research focus on the first two of three steps (53).

It is estimated that each human ovary contains more than two hundred and fifty thousand healthy follicles at birth with only 350-450 progressing to ovulation and more than ninety-five percent depleted by the time of menopause at 50±4 years due to natural degenerative processes (apoptosis) (53, 54,55). The individual oocytes begin maturation through a process of meiosis that arrests in the first prophase while becoming positioned within varying layers of somatic cells and forming the individual follicle stages summarized in Figure 11 below (52,55). The follicle stage classification is based on the general morphology of the granulosa cells (GC) surrounding the oocyte and follows a typical order of maturation to include primordial, primary, secondary, and antral follicles (53,54). Granulosa cell morphology and number of layers in each stage as originally described by Pedersen and Peters, with current and simplified versions adopted via Mishra and Luderer, and Gougeon, classify primordial follicles as having a single layer of flattened GCs, primary follicles as having a single layer of cuboidal or a combination of flattened and cuboidal in a single layer, secondary follicles as having multiple layers of cuboidal GCs, and antral follicles as having multiple layers of cuboidal GCs with an antral space containing follicular fluid not dissimilar to the composition of blood serum (6,53,75).

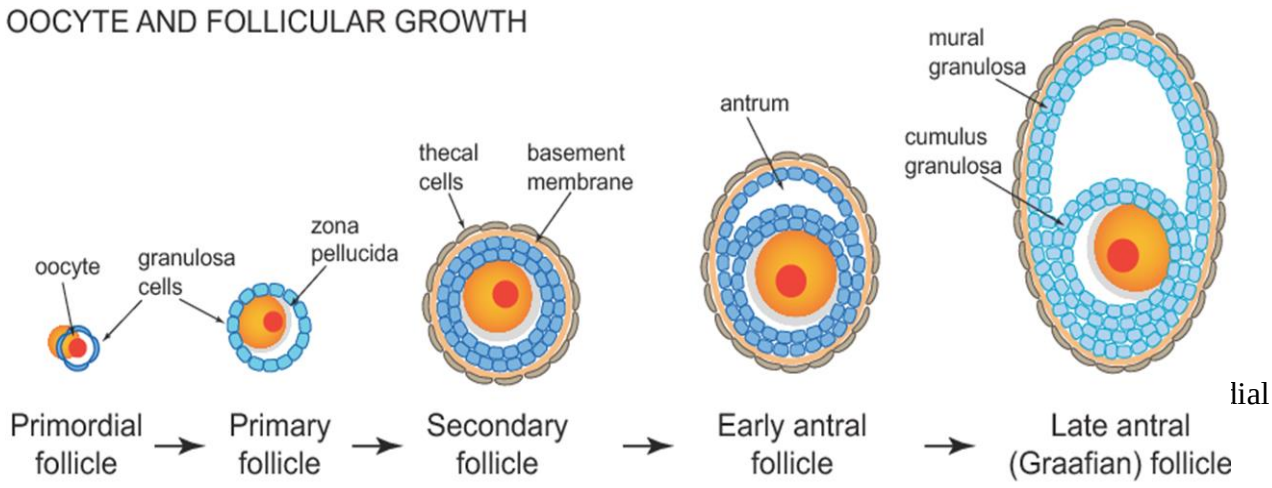

Figure 11: *Oocyte and follicular growth. Image credit: Clarke et al., 2017 (52).*

Studies and literature reviews have been conducted since the early-1900's regarding investigations of the biologic consequences of exposure to low LET IR (γ-rays and X-rays) from either environmental source, such as the atomic bomb and the Chernobyl accidents to ongoing research related to radiotherapy and other medical radiological exams (72). Our current data and understanding of IR exposures to the primary female reproductive organs, specifically related to the ovary, have primarily originated from various experiments in laboratory animals ranging from mice, rats, pigs, and even some canine species (71,72). The two major classes of general in vivo end points are classically defined as deterministic biological effects versus stochastic biological effects in which the former refers to effects that increase in severity in correlation to dose, such as teratogenicity, and in which the latter correlates to an increased risk with dose but without viable connection to severity of the outcome as would normally be consistent with carcinogenesis (71,72). According to Adriaens et al., the ED50 for a single dose X-ray sourced exposure to mouse and rat oocytes is 0.15Gy and 1Gy respectively and with increased radiosensitivity seen in earlier follicle stages (71). Unpublished data from the Luderer lab demonstrates that the ED50 for mouse follicle destruction by gamma-radiation is about 0.05 Gy. Wallace et al estimated that the ED50 for human primordial follicle destruction by gamma irradiation is <2 Gy (87). Sasaki et al. investigated dose-response relationships for solid ovarian tumor development after irradiation with single dose gamma radiation and X-rays in B6C3F mice and noted increased incidence and relative risk at dose ranges from 0.48-2.38Gy for induction of solid tumors (granulosa cell tumors, tubular adenomas, and luteal cell tumors) and noted similar studies with significant results utilizing doses as low as 0.16 Gy (70). The authors suggest an age-dependent relationship also exists in that effective dosing at a younger age also increases morbidity and mortality associated with carcinogenesis at any given dose when compared to adults (70).

In a further review by Adriaens et. al. the authors describe several broad categories of radiosensitivity end points to include cell killing, fertility, and genetic effects among several animal species (71).

The authors introduced the terminology of effective sterilizing dose (ESD) and defined it as the "fractionated dose at which premature ovarian failure occurs", noting corresponding low LET dose ranges in humans from 20.3Gy at birth to less than 14Gy for females at thirty years old (71). Interestingly, this data was utilized to guide relatively accurate prediction models for ovarian failure based on the above doses and patient ages (71). In research investigating medical procedures, patients undergoing treatment for gynecological cancers via fractionated doses of X-rays or γ-rays might be exposed to a dose range from around 40–60 Gy but spread over a prolonged period as a method to further reduce potential negative collateral effects on adjacent healthy tissues (50). Technological advances in the last decade have also introduced the concept of "FLASH-RT" in which ultra-high dose rates have shown promise for treatment protocols of equal efficacy with pronounced reductions in respective damage to adjacent healthy tissue (72). The challenges of appropriate risk modeling in a simple terrestrial environment have presented a complicated problem for researchers as technology continues to evolve and pathologic outcomes vary based on total dose of exposure, fractionation or single dose, dose rate, exposure source, age at the time of exposure, and biological effect dissimilarities between experimental species and human ovarian response.

In a recent review article entitled "Reproductive Hazards of Space Travel in Women and Men", Mishra and Luderer describe the additional dangers of the space environment and potential exposure of radiosensitive oocytes and adjacent granulosa or theca cells to high LET radiation previously defined as greater than 10KeV/μm (55). A major limitation in these past studies has been the duration of testing if performed in LEO or beyond the protective geomagnetic fields of the Earth. We are unaware of any studies investigating whole body or solid organ specific exposures to mixed GCRs and SEP that examined effects on the ovaries during a complete ovarian folliculogenesis cycle. Folliculogenesis from primordial to preovulatory follicles takes an estimated 50 days in rodents and 6 months in humans. An exposure of this duration would likely occur on a deep space mission to the moon or Mars (55).

Ground based or terrestrial studies could help to bridge this gap in knowledge by investigating comparisons of low vs. high LET exposure effects but are also limited and have historically investigated one ion (subcomponent of GCRs) at a time at dose rates greater than the estimated daily exposure inside of current model crewed capsules such as the Orion or Starliner (58). The ability to produce comparative terrestrial experimentation with HZE ions have also included new methods to better simulate GCR using mixed beam experiments, which involve exposure to multiple single ion species in quick succession cycling of single ion exposures at NASA's Space Radiation Research Laboratory (SRRL) at the Brookhaven National Laboratory (56,59).

It is accepted that high LET exposures likely create more complex ovarian damage when compared to similar doses of low LET exposures, evidenced by ICRP assigned 20:1 radiation weighting factor (WR) for heavy ions compared to terrestrial X-rays or γ-rays, but with mixed outcomes when looking at different endpoints such as follicular depletion or induction of ovarian tumors (50,55,60,61). Watanabe et al. investigated tumorigenicity of exposure of heavy ion (carbon) irradiation to B6C3F1 mice and noted lower induction of ovarian tumors at comparable respective X-ray doses of 50cGy and 5Gy, while studies published by Mishra et al. showed that irradiation of C57BL/6J mice with 50cGy charged heavy iron particles at 3 months of age resulted in prevalence of unilateral ovarian tumors in 47% and bilateral ovarian tumors in 7% of mice at 18 months of age, while controls had 14% prevalence of only unilateral tumors (55,61). The authors noted limitations in comparison to Watanabe and various other authors' work in the absence of direct low LET comparison dosing but noted the high LET exposure dose was within the ranges of other low LET studies looking at similar biological endpoints (55,61). Unexpected differences were even noted with utilization of different heavy ions constituting various LET's within the high LET ranges as in the Mishra et al. studies in which the ED50 for heavy oxygen ion exposure on primordial follicles was much lower than the respective value for heavy iron ion exposure using identical experimental protocols and suggesting increased potency for the former for this specific oocyte growth stage (6,62). In these studies by Mishra and Luderer

additional experiments examined the effects of charged oxygen and iron particles on different endpoints aimed at further elucidation of a proposed mechanistic model encapsulating the various types of damage induced by HZE particles in ovarian follicles (Figure 12) (6,54,62). The authors proposed that induction of ovarian tumors is likely related to early depletion of ovarian reserves and resulting increased concentrations of the gonadotropin hormones, LH and FSH due to lack of ovarian estrogen production, but that more research is needed to prove dose-response relationships based on the specific type of ionizing radiation exposure (54).

Finally, the above discussion considered measured effects of various dosing methods, doses, and sources of ionizing radiation exposure with end points measured primarily at the ovary, but did not discuss the known possibility of systemic effects potentially creating synergistic or other deleterious effects in the ovary due to damage incurred in other organ systems. In a study by Grover et al., in the J. of Ovarian Research 2018, the authors looked at a novel approach to targeted radiation dosing called the "Small Animal Radiation Research Platform" which allowed further investigations into histological differences at two weeks post-irradiation for differences in the damaging effects seen at the ovary when comparing whole-body irradiation and targeted organ or tissue specific dosing (94). The results did not reach statistical significance at the 1Gy dose level between total body irradiation and targeted dosing to the ovary but did exhibit a general trend in more compounding severe effects with total body irradiation (94). The authors concluded the study indicated a need for further investigations utilizing larger sample sizes and varied dosing levels to help elucidate any potentially significant differences in outcomes based on targeted versus whole body irradiation (94). If whole body radiation; as predominantly experienced in astronauts, was determined to create more severe downstream targeted ovarian effects at low doses compared to targeted exposure, then this data could be potentially utilized to further increase the accuracy of risk modeling via experimental designs aimed at elucidating contributory differences between the local and systemic effects. This additional data might also potentially help improve

ongoing research into mitigation strategies such as oral supplementation timing, dose, and ingredient combinations to reduce these effects during future prolonged deep space missions (92).

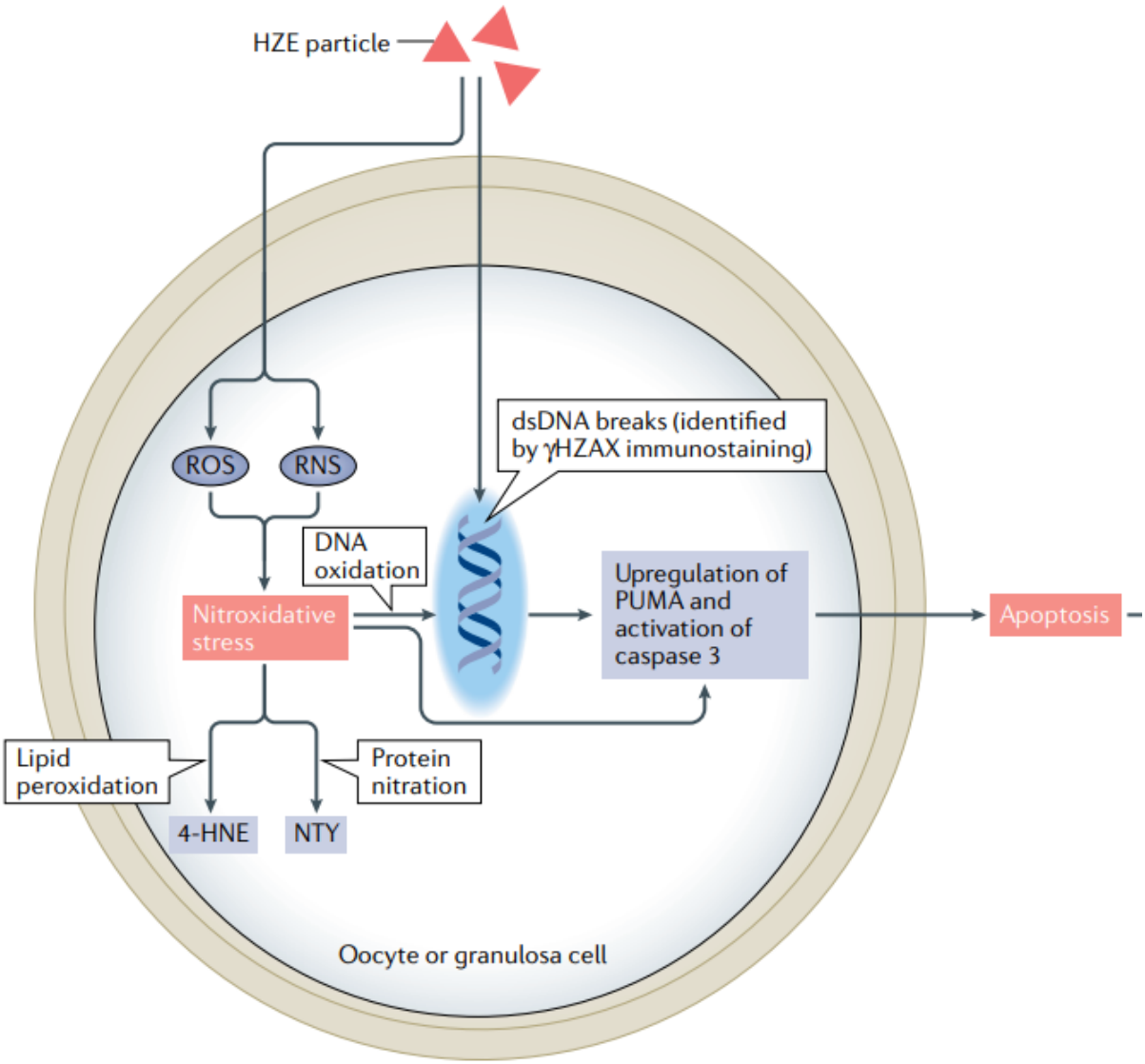

Figure 12: *Proposed mechanisms of HZE particle radiation-induced destruction of ovarian follicles. Image Credit Mishra and Luderer, 2019 (55).*

As previously discussed, exposure to IR causes multiple types of DNA damage in mammalian cells, the most severe being dsDNA breaks in a clustered pattern (72). A complex response to the detection of dsDNA breaks is quickly initiated by phosphorylation of a chromatin-based protein called H2ax by kinases such as ATM, ATR, and DNA-KPc to produce γ-H2AX at the site of the damage

(65,66,72). These newly phosphorylated histones constitute the first step in recruitment and activation of HR and NHEJ repair pathways and can be visualized utilizing immunofluorescence (IF) via primary and secondary antibodies to measure dsDNA damage. This damage can then be compared to equivalent exposure groups in the respective tissue but also may represent persistence or inability to effectively complete the various dsDNA repair pathways (65,66,72).

Exposures to HZE particles produce excess ROS and resultant lipid and protein damage. 4-Hydroxy-2-Nonenal (4-HNE) is a product of lipid oxidation, and 3-nitrotyrosine is a stable and subsequently identifiable marker for protein oxidation (31,68,69,85). IHC and IF protocols have been established and validated to allow additional characterization of experimental tissue data for evaluation of these IR related exposure end points. In the charged particle iron study, the researchers specifically measured characteristic dsDNA damage, oxidative lipid, and protein damage via IHC using 4-HNE, γ-H2AX, and nitrotyrosine antibodies respectively, but these inquiries were restricted to the exposure groups with doses of 0 and 50cGy (6). Similar studies by the same authors investigating charged oxygen particle exposure in vivo also showed dose dependent increases in dsDNA damage and oxidative lipid damage at doses ranging from 0 to 50cGy but without correlating γ-irradiated controls or additional IHC markers for protein damage (62).

Herein, I hypothesized that in vivo γ-radiation of mice dose-dependently increases dsDNA breaks and oxidative lipid damage in the ovaries at one week after irradiation and further that γ-radiation is a less potent inducer of these effects than charged iron or oxygen irradiation.

CHAPTER 2: METHODOLOGY

12-week-old C57BL/6J female mice were selected for this study. Animal experimental protocols were in accordance with the Guide for Care and Use of Laboratory Animals and approved by the Institutional Animal Care and Use Committee (IACUC) at University of California Irvine. These mice were restrained in 50mL conical tubes with air holes and exposed to whole-body γ-radiation at doses of 0, 0.15, and 0.5 Gy (total doses of 0, 15, and 50 cGy) at the UC Irvine Department of Radiation Oncology cesium 137 source (LET 0.8Kev/um). The dose rates were 0.0683 and 0.165 Gy/min delivered over 2.2 and 3.03 min, respectively, for the 0.15 and 0.5 Gy groups. The 0 Gy dose group mice were restrained similarly for 2 minutes without radiation. The subject mice were euthanized one week after exposure using carbon dioxide asphyxiation, and the ovaries with attached oviducts were dissected. One ovary was prepared in Bouin's fixative, processed, and stained with hematoxylin and eosin for ovarian follicle counts. The other ovary was fixed in 4% paraformaldehyde in phosphate buffered saline at 4°C overnight, then cryoprotected in 30% sucrose in PBS, embedded in Optimal Cutting Temperature (OCT) compound and stored at -80 °C until immunostaining.

Immunostaining and Immunofluorescence

Immunohistochemistry (IHC) using 4-Hydroxy-2-Nonenal (4-HNE) antibody (CAT#HNE-5, LOT#301718529) and immunofluorescence (IF) using phosphorylated histone H2AFX (γ-H2AX) (CAT#97185, LOT#17/21) and nitrotyrosine antibodies (CAT#06-284, LOT#3850438) were utilized to identify oxidative lipid damage, double-strand DNA breaks, and protein damage, respectively, and negative controls to include -/-, -/+, +/-, and IgG/+ were completed in concert to confirm absence of nonspecific staining for each specific protocol and antibody type (6,62,63,77). Luderer lab protocols

were utilized for IHC staining which included a two-day protocol with three technical replicates and n = 4 of each group for a total of 12 ovaries.

The first day of the IHC protocol was initiated via incubation of slides in 10mM citrate buffer for 20 minutes at 95°C followed by PBS washes and incubation for 15 minutes in Avidin D solution and Biotin solution respectively. The slides were then blocked with 10% goat blocking serum for 60 minutes at room temperature prior to application of primary antibody. The primary antibody was allowed to incubate for 24 hours at 4°C utilizing the Sequenza mounting system. Once completed, the slides were washed with PBS and incubated in 1:600 biotinylate anti-Rabbit Ig Reagent for 30 minutes at room temperature, washed in PBS, then incubated in 3% H_2O_2 for 10 minutes at room temperature. The slides were washed in PBS, then incubated in ABC reagent for another 30 minutes at room temperature. After completed, the slides were incubated with DAB substrate and peroxide buffer for 2 minutes, washed in PBS, then counterstained in filtered 4-fold diluted hematoxylin for 30 seconds. The remainder of the procedure involved tap water rinse, 0.4% HCL-95% EtOH rinse, and EtOH rinses from 95% to 100% (x3) for 3 minutes and 2 minutes respectively at room temperature. The slides were then equilibrated in Histo-clear (x2) for 3 minutes at room temperature and mounted with Omnimount solution using standard coverslips and allowed to cure 24 hours prior to scoring.

Immunofluorescence staining for γ-H2ax, NTY, and mouse vasa homolog (MVH) was performed via a four-day multiple antibody protocol adapted from Ansorg et al. for simultaneous use of two antibodies from the same host species with one technical replicate and n = 4 of each group for a total of 11 ovaries (80,82). The first day included antigen retrieval and started with slides washed in PBS solution then incubated in 10mM citrate buffer for 15min at 95°C. This followed by PBS wash then incubation in 5% goat blocking serum at room temperature for 1 hour. The slides were then incubated with the first primary antibody, rabbit anti-yH2AX/rabbit anti-NTY, diluted in blocking serum overnight at 4°C. Day two of the protocol included PBS washes followed by incubation of slides

in first secondary antibody, Alexa 633 goat anti-rabbit, for 1 hour at room temperature. The slides were then incubated in 10% normal rabbit serum for one hour at room temperature to ensure saturation of open paratopes from the first secondary antibody and then incubated in rabbit unconjugated monovalent Fab fragments overnight at 4°C. Day three of the protocol included incubation of the second primary antibody, MVH, diluted in 5% goat blocking serum overnight at 4°C. Day four included incubation of the slides in the second secondary antibody, Alexa 488 goat anti-rabbit, for 1 hour at room temperature. The slides were then incubated in Thermo-Fisher R37630 autofluorescence quenching agent in a 1:1:1 ratio of components A, B, and C for 3 minutes at room temperature. The slides were then incubated in 1:1000 solution of DAPI to stain nuclei for 5 minutes at room temperature, washed with PBS, then mounted with Thermo-Fisher P36980 mountant and cured overnight at room temperature. The slides were scored under UV excitation (400nm, 633nm).

Positivity for IHC and IF staining was scored blind to experimental group and defined in accordance with previously established standards in the Luderer laboratory as follows: Immuno-positive granulosa and theca cells demonstrated presence of staining and were classified according to stage of follicle development of the follicle in which they resided. Primordial and primary follicles with one or more positive granulosa cells were considered positive; secondary follicles with two or more positive granulosa or theca cells were considered positive, and antral follicles containing three or more positive granulosa or theca cells were considered positive. Healthy follicle immune-negative oocytes and granulosa cells were also counted, and the percentages of positive follicles of each follicle developmental stage were calculated for individual dose groups, and the reported means ± SEM are presented.

Statistical analyses

Statistical analysis was performed using SPSS 20 software and included Shapiro-Wilk and Kruskal-Wallis for non-parametric data.

CHAPTER 3: RESULTS

4-HNE immunostaining

Dose-dependent persistence of oxidative stress in the ovary at one week after exposure to low LET γ-radiation was measured via immunostaining for 4HNE (Figure 13). Mean positive percentage values (+/- SEM) were calculated based on radiation dose within the various follicular stages for both granulosa cells (GC) and oocytes (Figures 14,15). Positive percentage values were seen via GC immunostaining in primordial and primary follicles at the 0cGy and 15cGy dose groups, and in secondary follicles at the 15cGy dose groups. No antral follicles were identified at any dose group and no follicles were identified at the 50cGy dose group for any follicle stage. Positive percentage values were seen via oocyte immunostaining in primordial, primary, and secondary follicles in the 15cGy dose group, in primordial and primary in the 0cGy dose group, and in secondary stage at the 50cGy dose group. No antral follicles were identified via oocyte immunostaining for any dose group and no primordial or primary follicles were identified in the 50cGy dose group.

The data shows a nonsignificant positive dose-dependent increase in oxidative lipid damage for GC-positive primary and secondary follicles when directly comparing the 0cGy and 15cGy groups and a nonsignificant negative dose-dependent decrease in oxidative lipid damage for primordial follicles for the same two groups and for comparison of the 0cGy dose group from primordial to primary follicular stages. All dose groups with identified follicles for GC immunostaining descend to zero in secondary follicles apart from the 15cGy dose group. The data shows a nonsignificant positive dose-dependent increase in oxidative lipid damage for oocyte positive primordial and primary follicles when directly comparing the 0cGy and 15cGy groups.

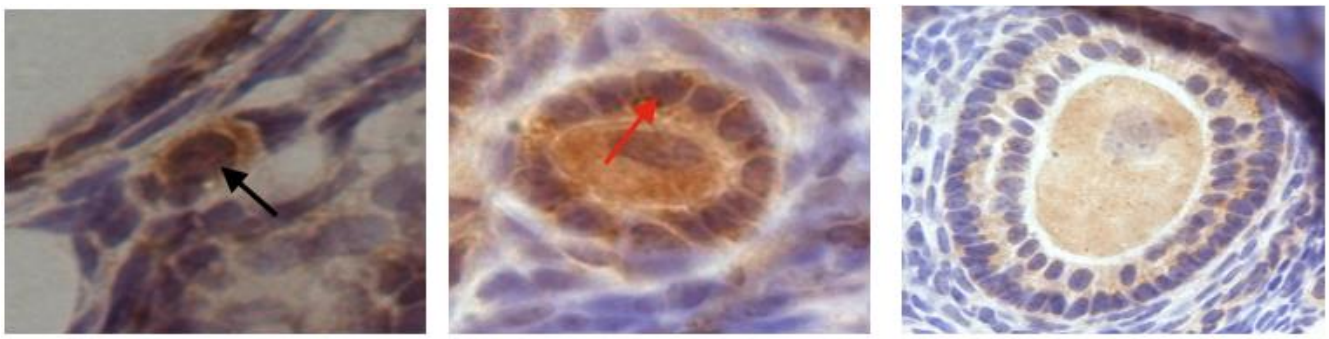

Figure 13: *Representative images of 4HNE positive immunostaining of granulosa cells (red arrow) and oocytes (black arrow) and example follicular maturation stages (left to right: Primordial (GAMOV-2 H1-4b, 0cGy), Primary (GAMOV-2 H10-4b, 15cGy), and Secondary (GAMOV-2 H11-4b, 15cGy).*

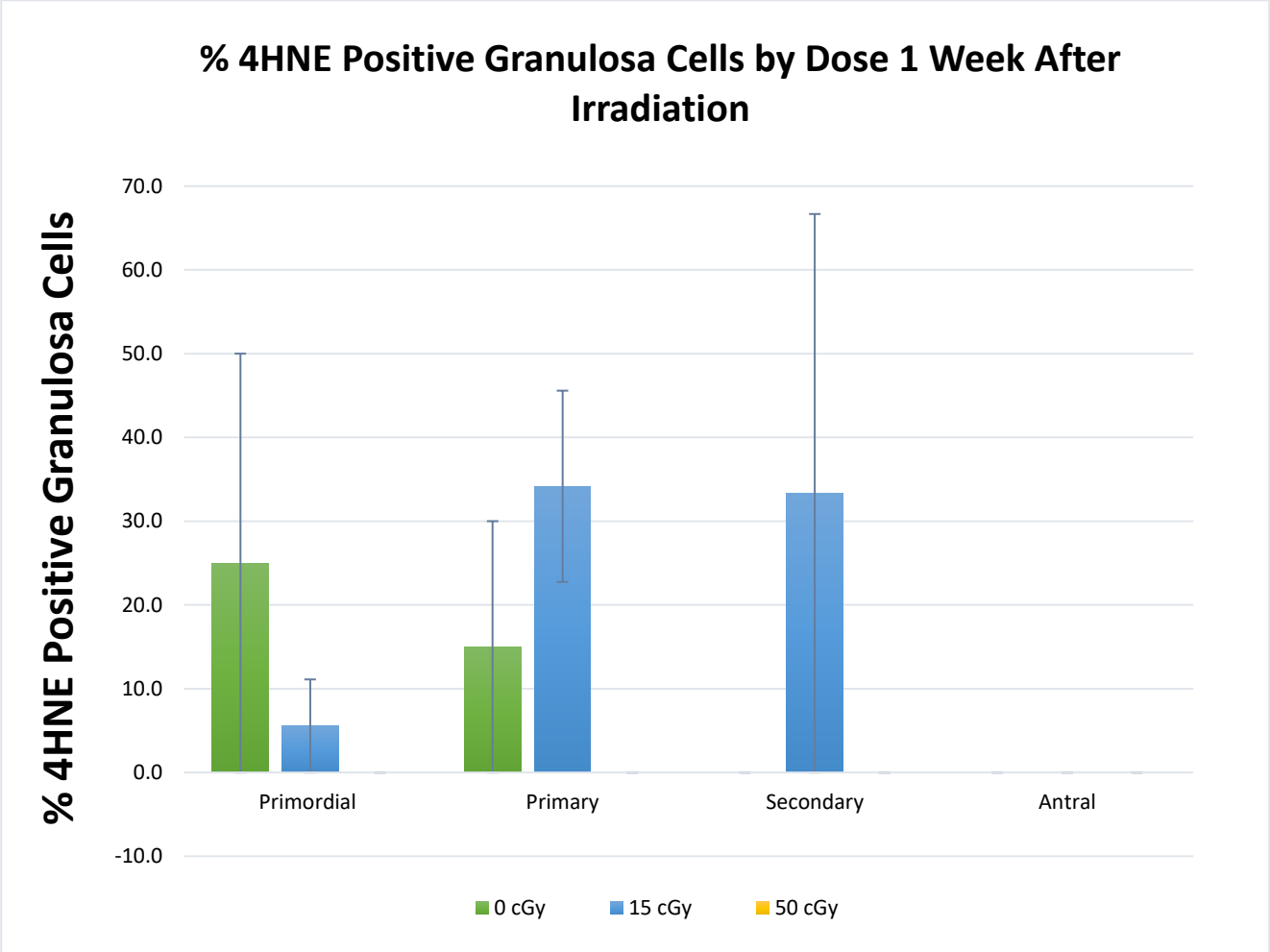

Figure 14: *Means+/- SEM percentages of follicles with 4HNE Positive Granulosa Cells by Dose 1 Week After irradiation Samples of immunostaining scored blind to treatment group; primordial (N=4 0cGy, N=3 15cGy, N=0 50cGy) and primary (N=4 0cGy, N=4 15cGy, N=0 50cGy) follicles with one or more positive granulosa cells, secondary follicles (N=3 0cGy, N=3 15cGy, N=0 50cGy) with two or more positive granulosa or theca cells, and antral follicles (N=0 all dose groups) containing three or more positive granulosa or theca cells.*

Interestingly, no oocytes were identified 4-HNE-positive in secondary follicles in the 0 cGy dose group and no antral follicles were identified in any dose group (Figure 15). There was a non-significant positive dose-dependent increase for 4-HNE-positive oocyte immunostaining at the secondary follicle stage when directly comparing the 15cGy and 50cGy dose groups at this follicular stage but with potential error calculations reaching as high as 100% of the magnitude of the data group.

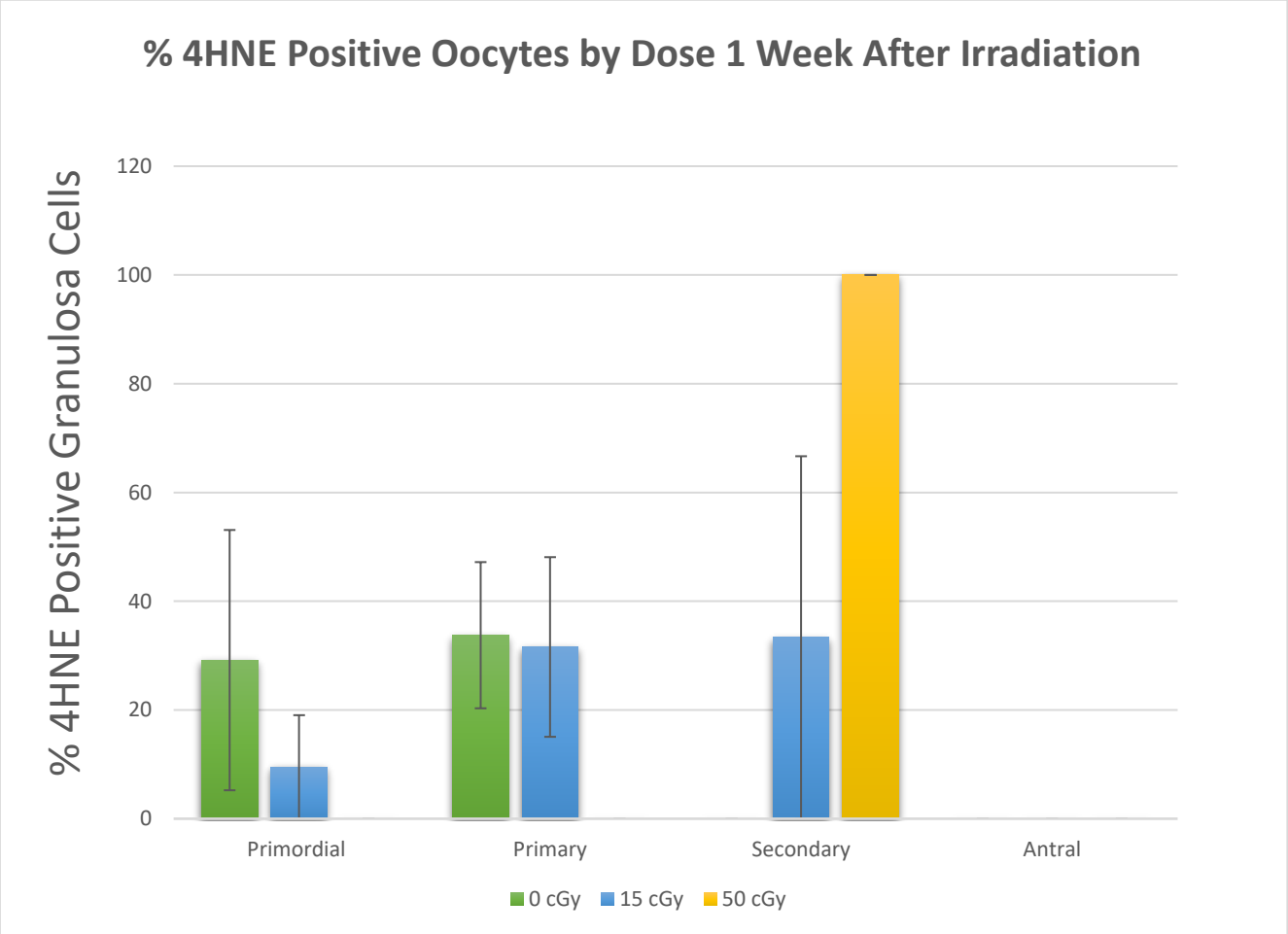

Figure 15: *Means+/- SEM percentages of follicles with 4HNE-positive oocytes by dose one week after irradiation. Samples of immunostaining scored blind to treatment group; primordial follicles (N=4 0cGy, N=3 15cGy, N=0 50cGy), primary follicles (N=4 0cGy, N=4 15cGy, N=0 50cGy), secondary follicles (N=3 0cGy, N=3 15cGy, N=1 50cGy), and antral follicles (N=0 all dose groups) counting oocytes (as positive or negative).*

It is noted via further statistical analysis that the standard error of the mean (SEM) for each stage and dose group for both GC and oocyte immunostaining were often as great in magnitude as the mean. Shapiro-Wilk and Kruskal-Wallis testing was completed with the former to verify lack of normality of

the data and the latter indicating p-values above the cutoff $p<0.05$ for significance of correlation of the means for each follicular maturity stage in both the GC and oocyte 4HNE immunostaining dose groups. Of note, the data did show a trend towards significance for the primary follicles with 4HNE-positive GCs ($p=0.06$).

γ-H2AX immunofluorescence

Persistence of double-strand DNA damage in the ovary at one week after low LET γ-irradiation for each stage of follicular development was assessed via immunofluorescence (IF) staining for γ-H2AX (Figure 16). Mean positive percentage values (+/- SEM) were calculated based on irradiation dose within the various follicular maturation stages for both GCs and oocytes (Figure 17,18). Significant positive percentage mean values based on GC IF were seen within the 0cGy dose group in primary follicle stages and nonsignificant positive percentage mean values in secondary follicle stages while the 15cGy dose group showed nonsignificant positive percentage mean values in primordial, secondary, and antral follicle maturation stages with no follicles identified in the primary stage. The 50cGy dose group scored via GC IF only showed nonsignificant mean positive percentage results in the secondary follicle stage and no follicles were identified in the primordial, primary, or antral stages for this does group.

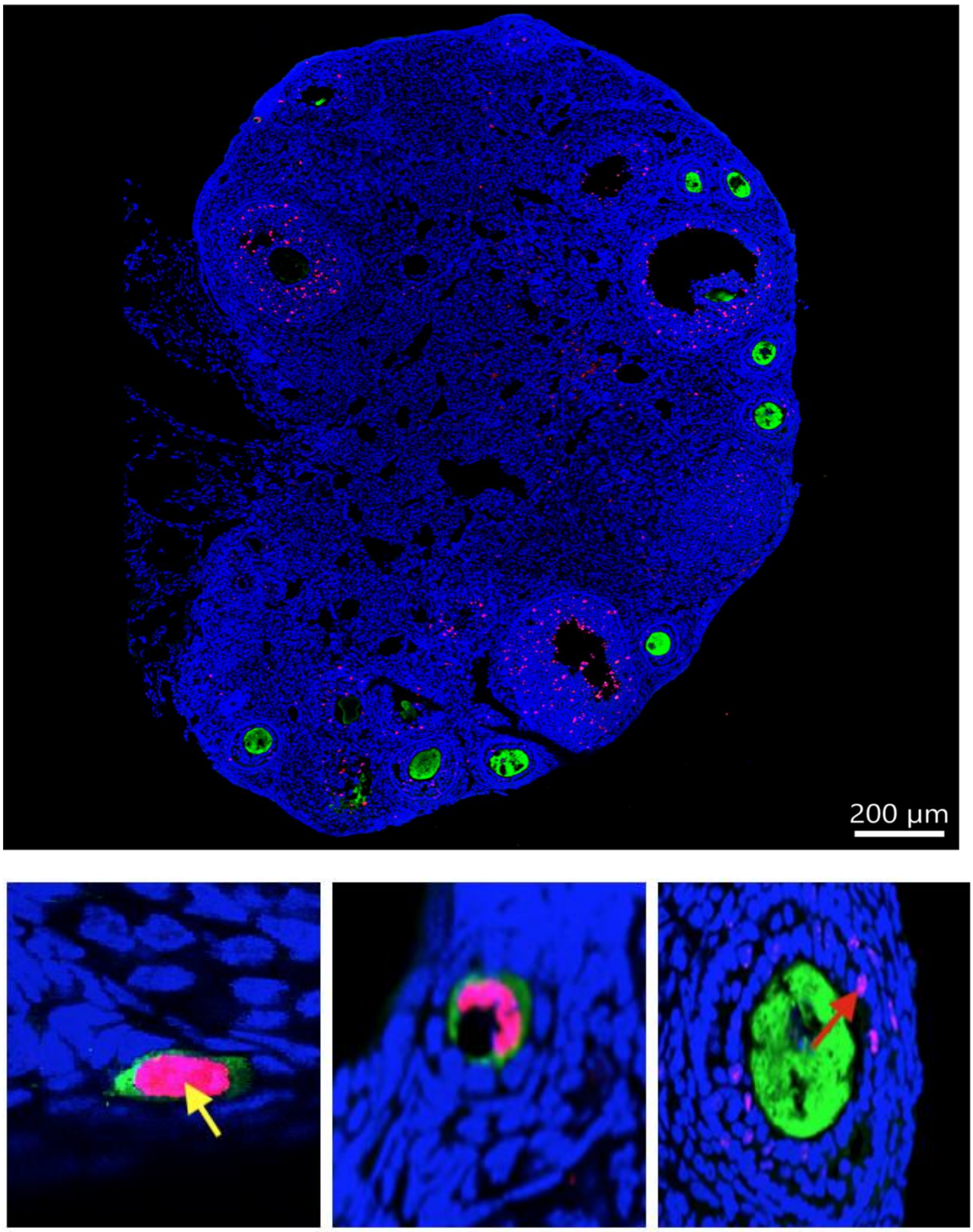

Figure 16: *Representative images (GAMOV-2 H12-4d, 15cGy group) of Y-H2AX positive immunofluorescence (pink) of granulosa cells (red arrow) and oocytes (yellow arrow) and example follicular maturation stages (left to right: Primordial, Primary, and Secondary). Green color is mouse VASA homolog immunofluorescence. Blue is nuclear staining with DAPI*

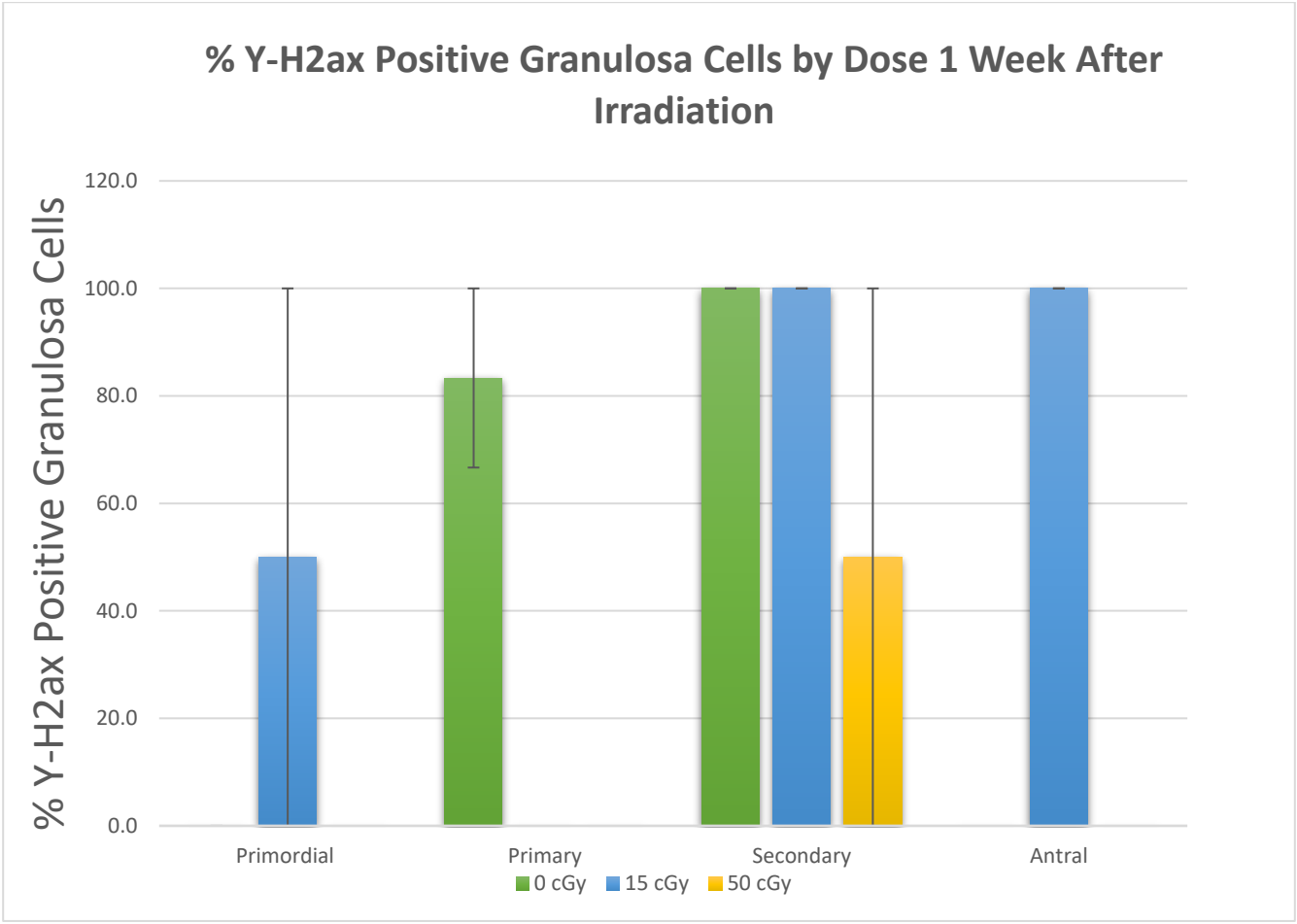

Figure 17: *Means+/- SEM percentages of follicles with Y-H2ax positive granulosa cells by dose one week after irradiation. Samples of immunostaining scored blind to treatment group; primordial follicles (N=3 0cGy, N=2 15cGy, N=0 50cGy) and primary follicles (N=3 0cGy, N=0 15cGy, N=0 50cGy) with one or more positive granulosa cells, secondary follicles (N=3 0cGy, N=4 15cGy, N=2 50cGy) with two or more positive granulosa or theca cells, and antral follicles (N=0 0cGy, N=2 15cGy, N=0 50cGy) containing three or more positive granulosa or theca cells.*

Mean γ-H2AX -positive percentage values for the 0cGy dose group grossly increased with maturity of follicle stage from primary to secondary. The 15cGy dose group noted the highest mean percent positive values at the secondary and antral stages elevated from 50% for the primordial group but without reaching statistical significance. SEMs for the GC IF immunostaining groups were smaller in comparison to the 4HNE dataset but also approached 100% of the mean in the 50cGy dose group at the secondary follicle stage.

Mean positive percentage values were seen via oocyte IF immunostaining in all follicle stages but also differed regarding dose groupings and only reached statistical significance for the positive primary follicle group (Figure 18). γ-H2AX -mean positive percentage values based on oocyte IF were seen within the 0cGy dose group in primordial, primary, and secondary follicular stages, while no antral follicles were identified for this dose group. The 15cGy group showed mean γ-H2AX-positive percentage values in the primordial, primary, secondary, and antral follicle groups and the 50cGy dose group showed mean positive percentage values in the secondary follicle group but none of these values reached statistical significance. No follicles were identified in the primordial, primary, or antral follicular maturation stages for the 50cGy dose group. Mean γ-H2AX -positive percentage values for the 0cGy and 15cGy dose groups grossly remained elevated in the primordial, primary, and secondary follicular stages. SEMs for the oocyte IF immunostaining groups were smaller in comparison to the 4HNE dataset but still approached 100% of the mean for the 50cGy dose group when scored and calculated for the secondary follicle stage.

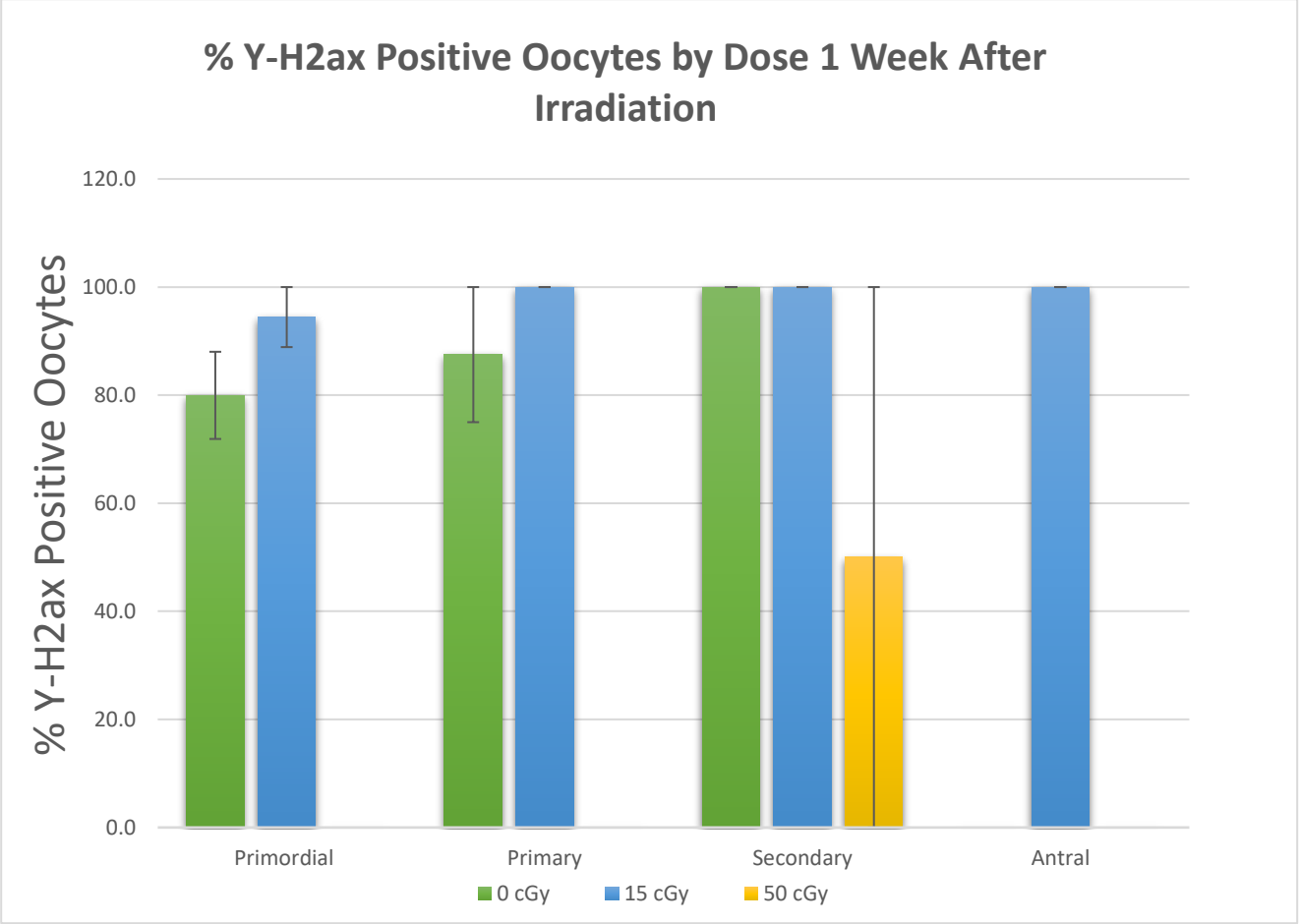

Figure 18: *Means+/- SEM percentages of follicles with e Y-H2ax-positive Oocytes by Dose One Week After Irradiation. Samples of immunostaining scored blind to treatment group; primordial follicles (N=4 0cGy, N=3 15cGy, N=0 50cGy) and primary follicles (N=4 0cGy, N=3 15cGy, N=0 50cGy), secondary follicles (N=3 0cGy, N=4 15cGy, N=2 50cGy), and antral follicles (N=0 0cGy, N=2 15cGy, N=0 50cGy) counting oocytes (as positive or negative).*

The 0cGy dose group showed a small increase percent γ-H2AX -positive value from primordial follicles to primary follicles, but then trended up in secondary follicles. The 50cGy dose group only showed nonsignificant percent mean γ-H2AX-positive results in the secondary follicle stage with zero follicles being identified for all the remaining stages. Shapiro-Wilk and Kruskal-Wallis testing were completed with both GCs and oocytes showing absence of normality and the distribution of percent mean γ-H2ax positive primary follicles based on GCs showing statistical significance between dosing groups (p=0.04, Kruskal-Wallis). Of note, the γ-H2ax IF percent mean positive results also did approach significance for both oocyte positive primordial and primary follicles respectively (p =0.086 & p=0.053, Kruskal-Wallis).

NTY immunofluorescence

Dose-dependent persistence of protein nitration in the ovary at one week for each stage of follicular development when exposed to low LET γ-radiation was investigated via immunofluorescence immunostaining for NTY (Figure 19). Optimization of the novel protocol noted positive results for the triple stain to include NTY, MVH, and DAPI, but technical iterations on the target tissue and duplicate positive control iterations from the "Heavy Oxygen Ion" irradiation study by Mishra and Luderer produced inferior quality results and were ultimately not able to be evaluated and scored for inclusion in this study (62).

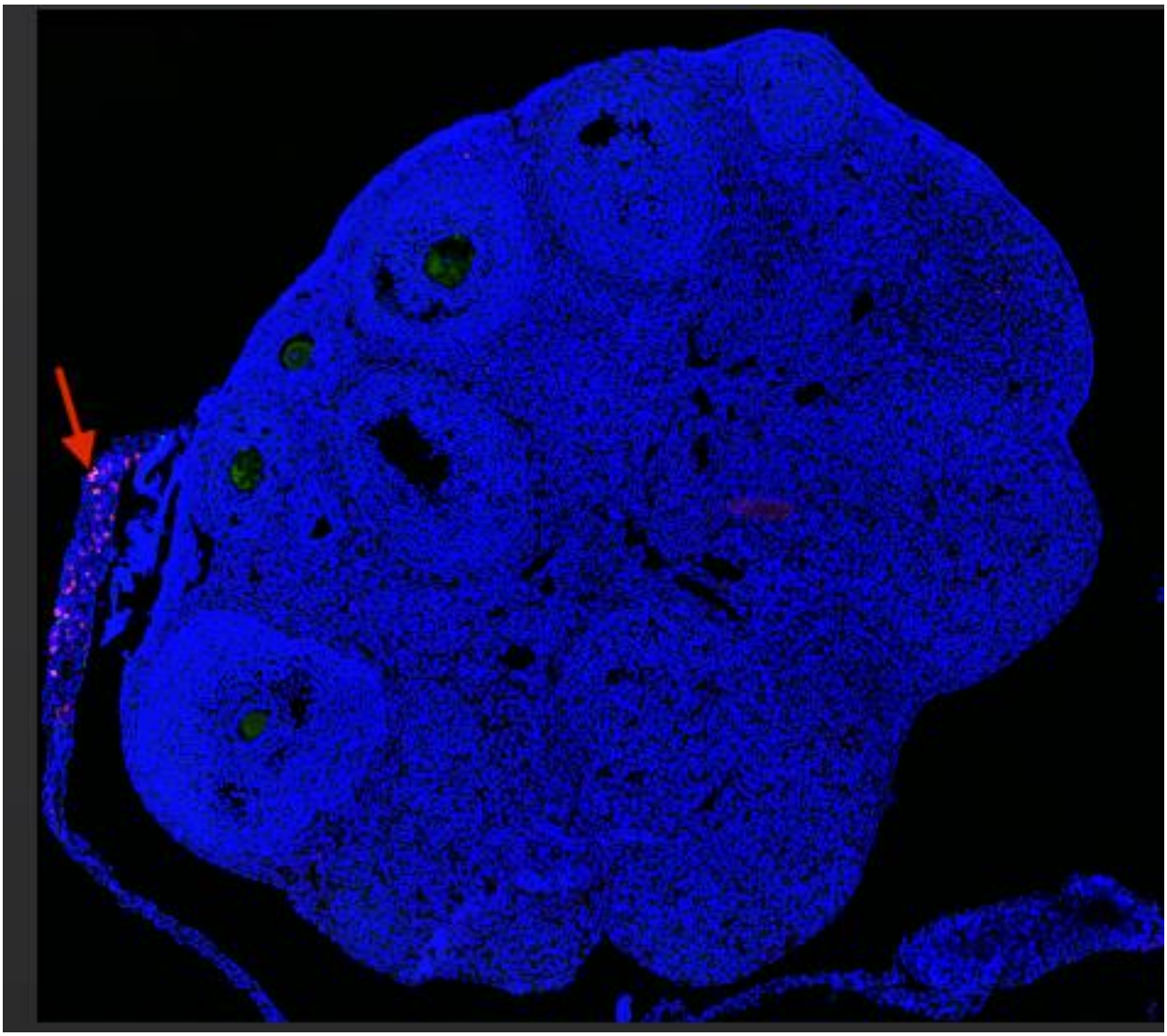

Figure 19: *Representative image of NTY (GG5 GAMOV1 5c) immunofluorescence immunostaining optimization iteration with positive staining in ovarian bursa (red arrow).*

CHAPTER 4: DISCUSSION

We undertook this study to build upon the limited body of knowledge from prior investigations of low LET γ-radiation-induced oxidative damage and DNA damage to ovarian follicles with focus on persistence of dose-related responses at each follicular stage one week after exposure. This study is the first that we are aware of that looked specifically at ovarian oxidative lipid, DNA, and protein damage at doses of 50cGy and lower, based on a proposed mechanistic model from Mishra and Luderer to explain potential downstream early ovarian failure and tumorigenesis (6,55,60). We hypothesized that we would see similar results to the prior Mishra and Luderer studies of both heavy oxygen and charged iron particles, with a positive linear dose-response relationship to all three markers, but with lower total values elicited from exposure to the lower LET radiation source and with doses selected above 15cGy (6,62,83).

We ultimately noted negative results when evaluating for oxidative lipid damage utilizing IHC staining for 4HNE at one-week post-irradiation. We hypothesized that γ-irradiation would likely follow the trends seen in the prior Mishra and Luderer studies and we would likely see a positive correlation to 4HNE staining with increased dose at most follicular stages (6,62). The percent positive values did show some positive dose-dependent increase in primary follicles for granulosa cells and secondary follicles for oocytes, but none of the values reached significance ($P > 0.05$). Interestingly, most of the samples at the 50cGy dose group were scored atretic in nearly every follicular maturity group and a single positive oocyte accounted for the greater than 100% positivity rate for the secondary follicle oocyte group at this dose level.

Similar results were noted in the 0cGy dose group for primordial follicles for both granulosa cells as well as oocytes due to recorded positive percent values that were greater than three times the values for the 15cGy group and with the raw data showing just a single positive follicle on a single section accounting for the entirety of the results in this dose group and oocyte maturity stage. A potential modification to improve the scoring, statistical analysis, and overall study design could be to evaluate all four sections on each slide; with care not to score larger follicles which would span multiple sections, to increase the number of scoreable follicles for each ovary and the overall power of the study for identifying significance for these end points. Oxidative injury from reactive oxygen species have been described in the research to accumulate due to normal cellular respiration and other endogenous processes in addition to external environmental stimuli such as exposure to gamma radiation or experiments with superovulation (78,81). These results, however, are inconsistent with what was observed in similar experiments with exposure to charged iron particles at both six hours and one-week post-irradiation and could represent possible errors in manual analysis, consistency of DAPI staining, or possible exaggerated positive percentages due to sample sizes within the raw data sets being too low for the respective dose groups (6,79). More research could possibly confirm the results by adding a 6-hr post-irradiation group, adding additional tissue samples to the technical iterations, including all tissue sections in the scoring of each slide, and adding additional dose groups at the 30cGy end point to increase the overall power of the study. Further improvements could also include stain intensity qualitative data in optimization steps or introducing an automated scoring process for this IHC protocol.

Investigation of the persistence of dsDNA breaks at one-week post low dose γ-irradiation by immunofluorescence staining for γ-H2ax and mouse vasa homolog (MVH) was performed via a multiple antibody protocol adapted from Ansorg et al. for simultaneous use of two antibodies for the same host species (80,82).

We hypothesized that the data would likely also support a positive correlation to dosing protocol in each of the oocyte maturation stages. The data showed nonsignificant results in both comparisons between individual dose groups and maturation stages of the oocyte as well as between different dose groups except for statistical significance in the primary follicles scored via granulosa cells.

For granulosa cells, we saw a nonsignificant positive dose-related increase in the 15cGy dose group for the primordial, secondary, and antral follicular stage with the most pronounced increase coming with scoring the secondary follicles which was also largely consistent with the results of oocyte scoring that included primary follicles. These results were inconsistent compared to the prior Mishra and Luderer iron particle study which resulted a positive, yet not quite significant dose dependent correlation in the 0cGy and 50cGy dose groups for secondary and antral follicle types when scored for γ-H2ax-positive granulosa cells and for primordial, secondary, and antral follicle types when scored for γ-H2ax-positive oocytes at one-week post-irradiation (6). Conversely, our study results showed several of the oocyte follicular stages had the highest mean percent γ-H2ax- positive scoring in the 0cGy group, and the 50cGy group had zero identified follicles for both granulosa cells and oocytes in all follicle types except for secondary follicles. The only group that achieved statistical significance ($p<0.04$) was for primary follicles with mean γ-H2ax-positive granulosa cells, which interestingly was absent of any identified follicles except for the 0cGy dose group. Possible discrepancies in comparison of the final data for these two studies could be due to an overly small data set via too few technical iterations and sections scored per slide, or technical differences when comparing results between two types of immunostaining techniques (IHC vs. IF). Additional data points at the one-week post-irradiation time point would likely help to further elucidate any dose and follicle related patterns and potentially help to achieve significance of the data in statistical comparisons between dose groups within each follicle type. It would also likely create a more accurate comparison by adding an additional data set to our study looking at the same immunostaining markers at the six-hour time point

while examining initial quantitative data of elevated dsDNA strand breaks that could explain differences seen at the later time point between the different LET sources of radiation.

Technical differences in the staining protocols utilized in the Mishra and Luderer studies and our study could introduce differences in results due to difficulties with 4HNE IHC manual scoring for the smaller primordial follicles and overall staining variance in all follicular stages between technical iterations (6,62). Immunofluorescence staining for γ-H2AX has the advantage of less difficulty in manual scoring of smaller primordial and primary follicles but presents with issues determining accuracy of overall positivity for all follicular stages in the setting of limited ability via dark-field microscopy to differentiate atretic vs. healthy follicles. This limitation could allow atretic positive follicles to be counted as healthy positive follicles skewing the data toward more positive percent values. To mitigate this, an alternate study design could include a positive control with the same tissues from the heavy iron study scored via IF for γ-H2ax or from our gamma irradiated tissues scored via IHC for γ-H2ax and compare the results.

Investigation of the persistence of oxidative damage to proteins at one-week after low dose γ-irradiation by immunofluorescence staining for NTY and MVH was performed utilizing a multiple antibody protocol adapted from Ansorg et al. for simultaneous use of two antibodies for the same host species (80,82). Unfortunately, as mentioned previously, this protocol yielded negative results for all tissue sections in all dose groups. An additional technical iteration was completed with positive control tissues from the Mishra and Luderer studies of both heavy oxygen particles and charged iron particles which also yielded similar negative results for all tissues in all dosing groups (6,62).

We believe that these results are likely due to a technical failure in the first primary antibody as multiple optimization technical iterations yielded appropriate results for the MVH oocyte stain, but with only limited peripheral positive staining occurring for NTY. Further optimization and technical iterations could be completed with a different antibody batch number to likely show positive scoring results at one-week post-irradiation in the different dose groups and follicle types as this was consistently seen in both the prior Mishra and Luderer studies via routine IHC staining (6,62).

CHAPTER 5: CONCLUSION

Radiation exposure risk assessment and stratification for female astronauts with specific concentration on ovarian toxicity continues to be a relatively understudied research topic but is critical in protecting these workers during proposed future missions to the lunar surface and deep space. Cucinotta et al. described, in detail, the challenges and need for further research on this topic by asking several fundamental questions relative to the possibility of accurately scaling HZE effects from γ-rays and determination of the linearity of effects from γ-rays at low dose rates (9). Mishra et al. successfully investigated multiple endpoints with two of the more common HZE particles which formed the basis for this study attempting to determine comparative results for several oxidative stress and dsDNA damage markers one week after γ-irradiation (6,62). Furthermore, this study attempted to introduce a combination immunofluorescence staining technique to the standard laboratory protocols for use with ongoing and future investigations.

We believe the newly developed immunofluorescence protocol, once optimized, will increase the accuracy of post-experimental analysis and specifically among smaller follicle counts. This will greatly increase the speed and reliability of data acquisition for these types of studies in the future. We also believe that our data and study design do not support persistence of increased oxidative stress and dsDNA damage at one week after gamma irradiation, in contrast to previous results of charged particle radiation studies in the Luderer lab. Further data are likely needed to increase the power of the study data and to elucidate any potential dose-response relationships before being utilized to develop critical RBE calculations to increase accuracy in risk assessment for future terrestrial mixed-beam studies with HZE particles.

REFERENCES

1. Fong, Kevin. “Moon Landing: Space Medicine and the Legacy of Project Apollo.” *The Lancet*, vol. 394, no. 10194, 2019, pp. 205–207., https://doi.org/10.1016/s0140-6736(19)31568-5.
2. Dunbar, Brian. “Artemis-I.” *NASA*, NASA, 29 Jan. 2018, https://www.nasa.gov/artemis-1.
3. “Orion.” *Lockheed Martin*, 25 Aug. 2022, https://www.lockheedmartin.com/en-us/products/orion.html?gclid=Cj0KCQjwyOuYBhCGARIsAIdGQROpRhvSdBQkKXC-exMUOjOIGSsgVLduVp6SsQJ9uBaD7N7IeLC_gFcaAvI5EALw_wcB.
4. Mars, Kelli. “5 Hazards of Human Spaceflight.” *NASA*, NASA, 27 Mar. 2018, https://www.nasa.gov/hrp/5-hazards-of-human-spaceflight.
5. Mars, Kelli. “NASA Astronauts Homepage.” *NASA*, NASA, 4 Jan. 2016, https://www.nasa.gov/astronauts.
6. Mishra, Birendra, et al. “Charged Iron Particles, Components of Space Radiation, Destroy Ovarian Follicles.” *Human Reproduction*, vol. 31, no. 8, 2016, pp. 1816–1826., https://doi.org/10.1093/humrep/dew126.
7. Cucinotta, Francis A, and Marco Durante. “Cancer Risk from Exposure to Galactic Cosmic Rays: Implications for Space Exploration by Human Beings.” *The Lancet Oncology*, vol. 7, no. 5, 2006, pp. 431–435., https://doi.org/10.1016/s1470-2045(06)70695-7.
8. Schimmerling, Walter. “Accepting Space Radiation Risks.” *Radiation and Environmental Biophysics*, vol. 49, no. 3, 2010, pp. 325–329., https://doi.org/10.1007/s00411-010-0286-0.
9. Cucinotta, Francis A. “A New Approach to Reduce Uncertainties in Space Radiation Cancer Risk Predictions.” *PLOS ONE*, vol. 10, no. 3, 2015, https://doi.org/10.1371/journal.pone.0120717.
10. Preston, D. L., et al. “Solid Cancer Incidence in Atomic Bomb Survivors: 1958–1998.” *Radiation Research*, vol. 168, no. 1, 2007, pp. 1–64., https://doi.org/10.1667/rr0763.1.
11. Margetta, Robert. “NASA Selects New Astronaut Recruits to Train for Future Missions.” *NASA*, NASA, 6 Dec. 2021, https://www.nasa.gov/press-release/nasa-selects-new-astronaut-recruits-to-train-for-future-missions.
12. Seedhouse, Erik. “Setting Acceptable Risk Levels for Astronauts.” *SpringerLink*, Springer International Publishing, 1 Jan. 1970, https://link.springer.com/chapter/10.1007/978-3-319-74615-9_3.
13. Turner, James E. *Atoms, Radiation, and Radiation Protec*^{ti}*on, 3rd, Completely Revised and ENL*. John Wiley & Sons, 2007.
14. Seedhouse, Erik. *Space Radiation and Astronaut Safety*. Springer International Publishing, 2018.
15. “Radiation Studie–: CDC - What Is Radiation?” *Centers for Disease Control and Prevention*, Centers for Disease Control and Prevention, 17 May 2022, https://www.cdc.gov/nceh/radiation/what_is.html.
16. *The Geomagnetic–Field - C/NOFS*. http://www.cnofs.org/Handbook_of_Geophysics_1985/Chptr04.pdf.

17. Cameron, J. “Radiation Dosimetry.” *Environmental Health Perspectives*, vol. 91, 1991, pp. 45–48., https://doi.org/10.1289/ehp.919145.

18. “Units of Ionising Radiation Measurement.” *ARPANSA*, https://www.arpansa.gov.au/understanding-radiation/what-is-radiation/radiation/measurement.

19. *Radiation and Its Health Effects | Nrc.gov*. https://www.nrc.gov/about-nrc/radiation/rad-health-effects.html.

20. Storer, John B., et al. “The Relative Biological Effectiveness of Various Ionizing Radiations in Mammalian Systems.” *Radiation Research*, vol. 6, no. 2, 1957, p. 188., https://doi.org/10.2307/3570599.

21. Furukawa, Satoshi, et al. “Space Radiation Biology for ‘Living in Space.’” *BioMed Research International*, vol. 2020, 2020, pp. 1–25., https://doi.org/10.1155/2020/4703286.

22. Thomas, D. J. “ICRU Report 85: Fundamental Quantities and Units for Ionizing Radiation.” *Radiation Protection Dosimetry*, vol. 150, no. 4, 2012, pp. 550–552., https://doi.org/10.1093/rpd/ncs077.

23. Schaefer, Hermann J., et al. “Atlas of Nuclear Emulsion Micrographs from Personnel Dosimeters of Manned Space Missions.” *DTIC*, https://apps.dtic.mil/sti/citations/ADA025970.

24. *Welcome to Baylor College of Medicine | BCM*. https://www.bcm.edu/sites/default/files/2020-05/red-risk-talk-g-nelson-042920.pdf.

25. Nelson GA. Fundamental space radiobiology. Gravit Space Biol Bull. 2003 Jun;16(2):29-36. PMID: 12959129.

26. Jia, Chengyou, et al. “The Role of DNA Damage Induced by Low/High Dose Ionizing Radiation in Cell Carcinogenesis.” *Exploratory Research and Hypothesis in Medicine*, vol. 000, no. 000, 2021, pp. 000–000., https://doi.org/10.14218/erhm.2021.00020.

27. Patel, Zarana S., et al. “Red Risks for a Journey to the Red Planet: The Highest Priority Human Health Risks for a Mission to Mars.” *Npj Microgravity*, vol. 6, no. 1, 2020, https://doi.org/10.1038/s41526-020-00124-6.

28. Martin, Lynn M., et al. “DNA Mismatch Repair and the DNA Damage Response to Ionizing Radiation: Making Sense of Apparently Conflicting Data.” *Cancer Treatment Reviews*, vol. 36, no. 7, 2010, pp. 518–527., https://doi.org/10.1016/j.ctrv.2010.03.008.

29. Cannan, Wendy J., and David S. Pederson. “Mechanisms and Consequences of Double-Strand DNA Break Formation in Chromatin.” *Journal of Cellular Physiology*, vol. 231, no. 1, 2015, pp. 3–14., https://doi.org/10.1002/jcp.25048.

30. Barnard, Stephen, et al. “The Shape of the Radiation Dose Response for DNA Double-Strand Break Induction and Repair.” *Genome Integrity*, vol. 4, no. 1, 2013, p. 1., https://doi.org/10.1186/2041-9414-4-1.

31. Wang, Hui, et al. “Hypoxic Radioresistance: Can Ros Be the Key to Overcome It?” *Cancers*, vol. 11, no. 1, 2019, p. 112., https://doi.org/10.3390/cancers11010112.

32. Wang, Hao, et al. “Cancer Radiosensitizers.” *Trends in Pharmacological Sciences*, vol. 39, no. 1, 2018, pp. 24–48., https://doi.org/10.1016/j.tips.2017.11.003.

33. Spence, Harlan E., et al. “Relative Contributions of Galactic Cosmic Rays and Lunar Proton ‘Albedo’ to Dose and Dose Rates near the Moon.” *Space Weather*, vol. 11, no. 11, 2013, pp. 643–650., https://doi.org/10.1002/2013sw000995.

34. “Department of Labor Logo United States Department of Labor.” *Ionizing Rad–ation - Background | Occupational Safety and Health Administration,* https://www.osha.gov/ionizing-radiation/background.

35. Matthiä, Daniel, et al. “A Ready-to-Use Galactic Cosmic Ray Model.” *Advances in Space Research*, vol. 51, no. 3, 2013, pp. 329–338., https://doi.org/10.1016/j.asr.2012.09.022.

36. K;, Cucinotta FA;Wu H;Shavers MR;George. “Radiation Dosimetry and Biophysical Models of Space Radiation Effects.” *Gravitational and Space Biology Bulletin : Publication of the American Society for Gravitational and Space Biology*, U.S. National Library of Medicine, https://pubmed.ncbi.nlm.nih.gov/12959127/.

37. Simpson, J A. “Elemental and Isotopic Composition of the Galactic Cosmic Rays.” *Annual Review of Nuclear and Particle Science*, vol. 33, no. 1, 1983, pp. 323–382., https://doi.org/10.1146/annurev.ns.33.120183.001543.

38. “Toxicological Profile for Ionizing Radiation.’ *ATSDR's Toxicological Profiles*, 2002, https://doi.org/10.1201/9781420061888_ch102.

39. “The Cell Cycle, Mitosis and Meiosis for Schools and Colleges.” *The Cell Cycle, Mitosis and Meiosis for Schools and Colleges | Virtual Genetics Education Centre | University of Leicester*, 10 Sept. 2020, https://le.ac.uk/vgec/topics/cell-cycle/the-cell-cycle-schools-and-colleges.

40. Cao, Lin-Lin, et al. “Histone Modifications in DNA Damage Response.” *Science China Life Sciences*, vol. 59, no. 3, 2016, pp. 257–270., https://doi.org/10.1007/s11427-016-5011-z.

41. Giglia-Mari, G., et al. “DNA Damage Response.” *Cold Spring Harbor Perspectives in Biology*, vol. 3, no. 1, 2010, https://doi.org/10.1101/cshperspect.a000745.

42. Weterings, Eric, and Dik C. Van Gent. “The Mechanism of Non-Homologous End-Joining: A Synopsis of Synapsis.” *DNA Repair*, vol. 3, no. 11, 2004, pp. 1425–1435., https://doi.org/10.1016/j.dnarep.2004.06.003.

43. Chang, Howard H., et al. “Non-Homologous DNA End Joining and Alternative Pathways to Double-Strand Break Repair.” *Nature Reviews Molecular Cell Biology*, vol. 18, no. 8, 2017, pp. 495–506., https://doi.org/10.1038/nrm.2017.48.

44. Moynahan, Mary Ellen, and Maria Jasin. “Mitotic Homologous Recombination Maintains Genomic Stability and Suppresses Tumorigenesis.” *Nature Reviews Molecular Cell Biology*, vol. 11, no. 3, 2010, pp. 196–207., https://doi.org/10.1038/nrm2851.

45. Thacker, John. “The rad51 Gene Family, Genetic Instability and Cancer.” *Cancer Letters*, vol. 219, no. 2, 2005, pp. 125–135., https://doi.org/10.1016/j.canlet.2004.08.018.

46. Li, Xuan, and Wolf-Dietrich Heyer. “Homologous Recombination in DNA Repair and DNA Damage Tolerance.” *Cell Research*, vol. 18, no. 1, 2008, pp. 99–113., https://doi.org/10.1038/cr.2008.1.

47. Gobbini, Elisa, et al. “Functions and Regulation of the MRX Complex at DNA Double-Strand Breaks.” *Microbial Cell*, vol. 3, no. 8, 2016, pp. 329–337., https://doi.org/10.15698/mic2016.08.517.

48. Kinner, A., et al. “-H2AX In Recognition and Signaling of DNA Double-Strand Breaks in the Context of Chromatin.” *Nucleic Acids Research*, vol. 36, no. 17, 2008, pp. 5678–5694., https://doi.org/10.1093/nar/gkn550.

49. *–ancer - How Tobacco Smoke Causes Disease: The B–Iogy ... - NCBI Bookshelf*. https://www.ncbi.nlm.nih.gov/books/NBK53010/.

50. Drago-Ferrante, Rosa, et al. "Extraterrestrial Gynecology: Could Spaceflight Increase the Risk of Developing Cancer in Female Astronauts? an Updated Review." *International Journal of Molecular Sciences*, vol. 23, no. 13, 2022, p. 7465., https://doi.org/10.3390/ijms23137465.

51. National Academies of Sciences, Engineering, and Medicine 2021. Space Radiation and Astronaut Health: Managing and Communicating Cancer Risks. Washington, DC: The National Academies Press. https://doi.org/10.17226/26155.

52. Clarke, H. "Figure 2.1 from Chapter 2 Control OfMammalian Oocyte Development by Interactions with the Maternal Follicular Environment: Semantic Scholar." *Figure 2.1 from Chapter 2 Control OfMammalian Oocyte Development by Interactions with the Maternal Follicular Environment | Semantic Scholar*, 1 Jan. 1970, https://www.semanticscholar.org/paper/Chapter-2-Control-ofMammalian-Oocyte-Development-by-Clarke-Clarke/3edf2fc83334543cc5024fbed9558fc907b2ad31/figure/0.

53. Gougeon, A. "Human Ovarian Follicular Development: From Activation of Resting Follicles to Preovulatory Maturation."'*Annales D'Endocrinologie*, vol. 71, no. 3, 2010, pp. 132–143., https://doi.org/10.1016/j.ando.2010.02.021.

54. Mishra, Birendra, et al. "Charged-Iron-Particles Found in Galactic Cosmic Rays Are Potent Inducers of Epithelial Ovarian Tumors." *Radiation Research*, vol. 190, no. 2, 2018, pp. 142–150., https://doi.org/10.1667/rr15028.1.

55. Mishra, Birendra, and Ulrike Luderer. "Reproductive Hazards of Space Travel in Women and Men." *Nature Reviews Endocrinology*, vol. 15, no. 12, 2019, pp. 713–730., https://doi.org/10.1038/s41574-019-0267-6.

56. Ronca, April E., et al. "Effects of Sex and Gender on Adaptations to Space: Reproductive Health." *Journa' of Women's Health*, vol. 23, no. 11, 2014, pp. 967–974., https://doi.org/10.1089/jwh.2014.4915.

57. Walsh, L., et al. "Research Plans in Europe for Radiation Health Hazard Assessment in Exploratory Space Missions." *Life Sciences in Space Research*, vol. 21, 2019, pp. 73–82., https://doi.org/10.1016/j.lssr.2019.04.002.

58. Gebhardt, Chris. "Crew Operations Training Gears up for Starliner and Orion." *NASASpaceFlight.com*, 16 Feb. 2023, https://www.nasaspaceflight.com/2023/02/starliner-orion-crew-preparations/.

59. La Tessa, Chiara, et al. "Overview of the NASA Space Radiation Laboratory." *Life Sciences in Space Research*, vol. 11, 2016, pp. 18–23., https://doi.org/10.1016/j.lssr.2016.10.002.

60. NITTA, Y., and M. HOSHI. "Relationship between Oocyte Apoptosis and Ovarian Tumours Induced by High and Low Let Radiations in Mice." *International Journal of Radiation Biology*, vol. 79, no. 4, 2003, pp. 241–250., https://doi.org/10.1080/0955300031000096315.

61. WATANABE, HIROMITSU, et al. "Comparison of Tumorigenesis between Accelerated Heavy Ion and X-Ray in B6C3F1 Mice." *Journal of Radiation Research*, vol. 39, no. 2, 1998, pp. 93–100., https://doi.org/10.1269/jrr.39.93.

62. Mishra, Birendra, et al. "Very Low Doses of Heavy Oxygen Ion Radiation Induce Premature Ovarian Failure." *Reproduction*, vol. 154, no. 2, 2017, pp. 123–133., https://doi.org/10.1530/rep-17-0101.

63. Barroso, Sonia I., and Andrés Aguilera. “Detection of DNA Double-Strand Breaks by γ-H2AX Immunodetection.” *Homologous Recombination*, 2020, pp. 1–8., https://doi.org/10.1007/978-1-0716-0644-5_1.

64. Kuo, Linda J., and Li-Xi Yang– “Γ-H2AX - A Novel Biomarker for DNA Double-Strand Breaks.” *In Vivo*, International Institute of Anticancer Research, 1 May 2008, https://iv.iiarjournals.org/content/22/3/305.short.

65. Collins, Patrick L., et al. “DNA Double-Strand Breaks Induce H2AX Phosphorylation Domains in a Contact-Dependent Manner.” *Nature Communications*, vol. 11, no. 1, 2020, https://doi.org/10.1038/s41467-020-16926-x.

66. Barroso, Sonia I., and Andrés Aguilera. “Detection of DNA Double-Strand Breaks by γ-H2AX Immunodetection.” *Homologous Recombination*, 2020, pp. 1–8., https://doi.org/10.1007/978-1-0716-0644-5_1.

67. *EPA*, Environmental Protection Agency, https://www.epa.gov/bmds.

68. Roede, James R., and Dean P. Jones. “Reactive Species and Mitochondrial Dysfunction: Mechanistic Significance of 4-Hydroxynonenal.” *Environmental and Molecular Mutagenesis*, 2010, https://doi.org/10.1002/em.20553.

69. Davies, Michael J. “The Oxidative Environment and Protein Damage.” *Biochimica Et Biophysica A–ta (BBA) - Proteins and Proteomics*, vol. 1703, no. 2, 2005, pp. 93–109., https://doi.org/10.1016/j.bbapap.2004.08.007.

70. SASAKI, SHUNSAKU, and NOBUO FUKUDA. “Dose-Response Relationship for Induction of Solid Tumors in Female B6C3F1 Mice Irradiated Neonatally with a Single Dose of Gamma Rays.” *Journal of Radiation Research*, vol. 40, no. 3, 1999, pp. 229–241., https://doi.org/10.1269/jrr.40.229.

71. Adriaens, I., et al. “The Current Knowledge on Radiosensitivity of Ovarian Follicle Development Stages.” *Human Reproduction Update*, vol. 15, no. 3, 2009, pp. 359–377., https://doi.org/10.1093/humupd/dmn063.

72. Friedl, Anna A., et al. “Radiobiology of the Flash Effect.” *Medical Physics*, vol. 49, no. 3, 2021, pp. 1993–2013., https://doi.org/10.1002/mp.15184.

73. “Reproduction and Fertility.” *Society for Reproduction and Fertility*, https://srf-reproduction.org/reproduction-and-fertility/.

74. Lopez, Sarah G, and Ulrike Luderer. “Effects of Cyclophosphamide and Buthionine Sulfoximine on Ovarian Glutathione and Apoptosis.” *Free Radical Biology and Medicine*, vol. 36, no. 11, 2004, pp. 1366–1377., https://doi.org/10.1016/j.freeradbiomed.2004.02.067.

75. PEDERSEN, T., and H. PETERS. “Proposal for a Classification of Oocytes and Follicles in the Mouse Ovary.” *Reproduction*, vol. 17, no. 3, 1968, pp. 555–557., https://doi.org/10.1530/jrf.0.0170555.

76. Canning, Jacqueline, et al. “Evidence for Genetic Modifiers of Ovarian Follicular Endowment and Development from Studies of Five Inbred Mouse Strains.” *Endocrinology*, vol. 144, no. 1, 2003, pp. 9–12., https://doi.org/10.1210/en.2002-220988.

77. Lim, Jinhwan, et al. “Glutathione-Deficient Mice Have Increased Sensitivity to Transplacental Benzo[a]Pyrene-Induced Premature Ovarian Failure and Ovarian Tumorigenesis.” *Cancer Research*, vol. 73, no. 2, 2013, pp. 908–917., https://doi.org/10.1158/0008-5472.can-12-3636.

78. Reeg, Sandra, and Tilman Grune. “Protein Oxidation in Aging: Does It Play a Role in Aging Progression?” *Antioxidants & Redox Signaling*, vol. 23, no. 3, 2015, pp. 239–255., https://doi.org/10.1089/ars.2014.6062.

79. Podszun, Maren C., et al. “4-HNE Immunohistochemistry and Image Analysis for Detection of Lipid Peroxidation in Human Liver Samples Using Vitamin E Treatment in NAFLD as a Proof of Concept.” *Journal of Histochemistry & Cytochemistry*, vol. 68, no. 9, 2020, pp. 635–643., https://doi.org/10.1369/0022155420946402.

80. Ansorg, Anne, et al. “Immunohistochemistry and Multiple Labeling with Antibodies from the Same Host Species to Study Adult Hippocampal Neurogenesis.” *Journal of Visualized Experiments*, no. 98, 2015, https://doi.org/10.3791/52551.

81. Nie, Xiaowei, et al. “Establishment of a Mouse Model of Premature Ovarian Failure Using Consecutive Superovulation.” *Cellular Physiology and Biochemistry*, vol. 51, no. 5, 2018, pp. 2341–2358., https://doi.org/10.1159/000495895.

82. Song, Kunkun, et al. “Expression Pattern of Mouse Vasa Homologue (MVH) in the Ovaries of C57BL/6 Female Mice.” *Medical Science Monitor*, vol. 22, 2016, pp. 2656–2663., https://doi.org/10.12659/msm.899830.

83. Shah, D J, et al. “Radiation-Induced Cancer: A Modern View.” *The British Journal of Radiology*, vol. 85, no. 1020, 2012, https://doi.org/10.1259/bjr/25026140.

84. “Types of Ionizing Radiation.” *Types of Ionizing Radiation [MOE]*, https://www.env.go.jp/en/chemi/rhm/basic-info/1st/01-03-03.html.

85. Xiao, Mengqing, et al. “Pathophysiology of Mitochondrial Lipid Oxidation: Role of 4-Hydroxynonenal (4-HNE) and Other Bioactive Lipids in Mitochondria.” *Free Radical Biology and Medicine*, vol. 111, 2017, pp. 316–327., https://doi.org/10.1016/j.freeradbiomed.2017.04.363.

86. “Dou–le+Helix - NASA Search Results.” *NASA*, NASA, https://nasasearch.nasa.gov/search/images?affiliate=nasa&query=double%2Bhelix.

87. Wallace, W.H.B., et al. “The Radiosensitivity of the Human Oocyte.” *Human Reproduction*, vol. 18, no. 1, 2003, pp. 117–121., https://doi.org/10.1093/humrep/deg016.

88. Pawlik, Timothy M., and Khandan Keyomarsi. “Role of Cell Cycle in Mediating Sensitivity to Radiotherapy.” *International Journal of Radiation Oncology*Biology*Physics*, vol. 59, no. 4, 2004, pp. 928–942., https://doi.org/10.1016/j.ijrobp.2004.03.005.

89. Powathil, Gibin G., et al. “Towards Predicting the Response of a Solid Tumour to Chemotherapy and Radiotherapy Treatments: Clinical Insights from a Computational Model.” *PLoS Computational Biology*, vol. 9, no. 7, 2013, https://doi.org/10.1371/journal.pcbi.1003120.

90. Ruiz-Herrera, Aurora, et al. “Radiobiology and Reproduction—What Can We Learn from Mammalian Females?” *Genes*, vol. 3, no. 3, 2012, pp. 521–544., https://doi.org/10.3390/genes3030521.

91. Devi, P.Uma, and A Kumar. “Radiosensitivity Changes during Oocyte Growth in Mouse: An Analysis of the Contributing Factors.” *Medical Hypotheses*, vol. 8, no. 5, 1982, pp. 473–476., https://doi.org/10.1016/0306-9877(82)90007-x.

92. Prasad NK, Kim HJ (2021) Attenuation of Space Radiation-Induced Damage by an Oral Supplementation with a Mixture of Micronutrients in Astronauts. J Med Phys and Appl Sci Vol.6 No.5: 11.

93. Kuefner, Michael A., et al. “Effect of Antioxidants on x-Ray–Induced γ-H2AX Foci in Human Blood Lymphocytes: Preliminary Observations.” *Radiology*, vol. 264, no. 1, 2012, pp. 59–67., https://doi.org/10.1148/radiol.12111730.

94. Grover, Allison R., et al. “Use of a Small Animal Radiation Research Platform (SARRP) Facilitates Analysis of Systemic versus Targeted Radiation Effects in the Mouse Ovary.” *Journal of Ovarian Research*, vol. 11, no. 1, 2018, https://doi.org/10.1186/s13048-018-0442-8.